

Geochemical characteristics of basalts from Andaman subduction zone: Implications on magma genesis at intraoceanic back arc spreading centres

Abhishek Saha*, Abhay V. Mudholkar, K.A. Kamesh Raju, Bhagyashree Doley, Simontini Sensarma

CSIR-National Institute of Oceanography, Dona Paula, Goa 403 004, India

*E-mail: asaha@nio.org

Abstract

This study reports new petrological and geochemical data for the ocean floor volcanic rocks dredged from the back arc basin of Andaman Sea and elucidates their geochemical characteristics and petrogenetic aspects to provide insights into the melt generation processes, oceanic crust emplacement and tectonomagmatic evolution of the Andaman back arc basin. The studied samples are porphyritic basalts with olivine, plagioclase and clinopyroxene representing the phenocrystal and the groundmass composition marked by plagioclase microlites, granular clinopyroxenes, and glass. Geochemical characteristics of these basalts reflect sub-alkaline, tholeiitic composition of precursor magma that experienced clinopyroxene-Ti magnetite fractionation. The overall geochemical trend for these basalts reflects LILE-HFSE-REE depleted MORB-type chemistry which is modified by input from subduction-derived components.

Pronounced enrichment in selected LREE (Nd) and incompatible fluid-mobile trace elements like Ba with positive primitive mantle normalized La and Sr anomalies in majority of these basalts are attributed to transport and influx of slab-dehydrated fluids and sediments into the depleted back arc mantle asthenosphere from the dehydrating subducted oceanic lithosphere in volcanic arc front during initial stage of back-arc rifting in the Andaman Sea. The studied basalts were derived by 10%-30% partial melting of a heterogeneous spinel lherzolitic mantle at a shallow depth. The chemical heterogeneity of the spinel lherzolite source suggest a enrichment-depletion history of back arc mantle correlatable with the transitional tectonic evolution of the back arc basin from an initial rifting to matured spreading stage. The depleted MORB type mantle (DMM) beneath a juvenile back arc experienced infiltration of fluids and subduction-derived components (SDC) from proximal subducting oceanic slab that gradually diminished with increasing distance from the arc and progressive back arc spreading. The episodes of melt generation and magma genesis invoke a gradual geodynamic transition from incipient back arc rifting to matured back arc spreading stages in the tectono-magmatic evolution of the Andaman back arc basin system. Oceanic crust generated during the incipient rifting stage sampled arc-type melts enriched and hydrated by subduction inputs and fluid flux, while oceanic crust formed during matured back arc extension stage inherited trace element depleted MORB-type mantle signatures devoid of subduction influence.

Keywords: Andaman Sea; Back arc basin; Depleted mantle; Slab-dehydrated fluids; Rifting to spreading

1. Introduction

The thermal and chemical conditions required for melt generation in mantle asthenosphere are primarily governed by the convective cycle in the mantle and the tectonic processes operative in different plate margins across the globe. This includes (i) divergence of oceanic lithosphere ensued by upward advection and decompression melting of depleted mantle material, melt extraction resulting a refractory residue (ii) subduction of oceanic lithosphere and partial melting of sub-arc mantle wedge triggered by infiltration of slab-dehydrated fluids and influx of subduction-derived components (Hofmann, 1997; Martinez and Taylor, 2002; Niu and O'Hara, 2009; Saha *et al.*, 2018). The petrological and geochemical characteristics of juvenile oceanic crust formed at mid oceanic ridge (MOR) systems and marginal back arc basins (BAB) are progressively influenced by variable extents of magmatic input, seawater interaction, hydrothermal alteration and tectonic activities during its horizontal movement towards convergent plate margins (Jourdain *et al.*, 2016; Inglis *et al.*, 2017). Melt extraction and mantle depletion processes at MORs and BABs with flux-induced metasomatic enrichment of mantle at ocean-ocean and ocean-continent convergent margins collectively attribute to the pervasive chemical heterogeneity in the asthenospheric mantle triggering magmatism of diverse compositions. A geochemically depleted asthenospheric mantle rendered by melt extraction episodes at mid oceanic ridge (MOR) systems and back arc basins (BAB) is re-injected and replenished at ocean-ocean and ocean-continent subduction zones by hydration, metasomatism and hybridization of asthenospheric mantle wedge through release of fluids, sediments and melts from dehydration and melting of subducting oceanic slab respectively (Masuda and Fryer, 2015; Brandl *et al.*, 2017; Inglis *et al.*, 2017). Magmas produced in mid oceanic ridge settings and island arc systems reflect distinct geochemical features that links respective magmatic processes and geodynamic conditions. The mid oceanic ridge basalts (MORB) are typified by depleted incompatible trace element compositions indicating their origin from decompression melting of upwelling refractory sub-ridge mantle in response to oceanic plate divergence; while the island arc basalts (IAB) are marked by elevated abundances of large ion lithophile elements (LILE) and depleted high field strength elements (HFSE) relative to MORB thereby finger printing flux melting induced by interaction and elemental exchange between subducting oceanic lithosphere and overlying mantle wedge (Tatsumi and Eggins, 1995; Elliott *et al.*, 1997; Pearce and Stern, 2006; Keller *et al.*, 2008, Manikyamba *et al.*, 2016). However, the geochemical signatures of magmas generated in back arc basins are transitional between MORB and IAB. In general, back arc basin basalts (BABB) show hydrous (2.5 wt. %H₂O), LILE enriched-HFSE depleted compositions and these geochemical attributes implicate significant control of the subducting oceanic lithosphere and

mantle wedge on the back-arc spreading processes, fluid gradients, element transport and magma supply beneath back-arc mantle (Martinez and Taylor, 2002; Fryer *et al.*, 1990; Stolper and Newman, 1994; Langmuir *et al.*, 2006; Kelly *et al.*, 2006). Incipient back arc basins developed proximal to the arc show pronounced subduction signatures, whereas the influence of subduction components gradually diminish with increasing distance from the arc front towards matured back arc basin distal from the arc. Therefore, melt generation, geochemical variations and petrogenetic evolution in BAB can be accounted in terms of (i) distance from the volcanic arc front (ii) asthenospheric and subduction input into the back arc mantle (iii) influence of subducting oceanic slab and extent of fluid/volatile flux (iv) mixing between MOR and arc mantle (v) lateral variations in upper mantle temperatures and (vi) melting conditions and fractionation of the melt during its ascent to the ocean floor (Lee and Wada, 2017; Pearce and Stern, 2006; Wiens *et al.*, 2006; Keller *et al.*, 2008).

Back arc spreading centres across the globe including Mariana, Tonga, East Scotia, Lau and Manus back arc basins are characterized by slow (<50 mm/yr) to fast (>100mm/yr) spreading rates with extensional axes at 10 km to 400 km behind the volcanic arcs thereby exhibiting variable geochemical compositions of back arc lavas deriving from depleted MORB-like and enriched, hydrated, arc-like mantle sources. A MORB-type oceanic crust is generated where spreading axis is distal from the arc and subducted slab, while an arc-type oceanic crust forms when the extensional axis lies proximal to the subduction zone (Taylor and Martinez, 2003). The intraoceanic arc-back arc system in the Andaman Sea represents an actively opening back arc spreading centre and potential site of juvenile oceanic crust generation in the northeast Indian Ocean. The Andaman back-arc basin has been tectonically modified by the ongoing subduction of Indian plate and spreading in the Andaman seafloor (Kamesh Raju *et al.*, 2004; Curray, 2005). Though significant geophysical surveys have been extensively carried out so far, however, petrological and geochemical studies of back arc basin basalts from Andaman Sea are less attended and yet of immense importance to understand the tectonomagmatic processes influencing the petrogenetic evolution of oceanic crust in an active back-arc basin. This study reports new petrological and geochemical data for the submarine volcanic rocks dredged from Andaman back arc basin and aims to understand their petrogenesis, mantle processes, melting conditions and tectonic control on melt generation.

2. Geological Setting

In the northeast Indian Ocean, the subduction of Indian plate beneath the Southeast Asian plate initiated following the Gondwanaland breakup, during the early Cretaceous. This major tectonic event marked the formation of the Indo-Burma range and the Andaman island arc-trench system

comprising the Andaman-Nicobar islands and Andaman back-arc basin (Rao *et al.*, 1996). Geophysical studies including bathymetric, magnetic, gravimetric, heat flow and seismic surveys have collectively suggested active ocean floor spreading and opening of the Andaman Sea commencing at 4 Ma at a full rate of 16mm/yr, increasing to 38 mm/yr from 2.5-2 Ma to present classifying it as a slow-spreading ridge – rift system with a westward propagation (Kamesh Raju *et al.*, 2004; Curray, 2005; Diehl *et al.*, 2013; Jourdain *et al.*, 2016). The Andaman Basin extends from Myanmar in the north to Sumatra in the south and from Malay Peninsula in the east to Andaman and Nicobar islands in the west with prominent morphological features including the Nicobar deep, Barren-Narcondam volcanic islands, Invisible bank, and Alcock and Sewell seamount complexes. The back arc spreading centre located at the Andaman Sea basin is characterized by a ~12 km-wide valley, and a flat-lying valley floor at 3600 m water depth sedimented by the Irrawaddy River system in Myanmar (Rao *et al.*, 1996).

The active opening of the marginal back arc basin in the Andaman Sea is primarily governed by the oblique convergence of the Indian-Australian plate beneath the western Sunda arc thereby separating the Burmese sliver plate to the northwest from the Sunda plate to the southwest. This oblique plate convergence resulting in the back arc extension of the Andaman Sea is in contrast to the trench rollback controlled extensions in south western Pacific back-arc basins and involves a transtensional mode of back arc spreading and oceanic crust generation also referred to as leaky transform (Lodolo *et al.*, 2013).

Multi-beam swath bathymetry (Rao *et al.*, 1996; Kamesh Raju *et al.*, 2004) exhibits complex topography of the Central Andaman Basin comprising of an active back-arc spreading centre with well-defined rift valley at the centre and several seamounts that form a chain parallel to the island arc system (Rao *et al.*, 1996). The back-arc spreading centre trends NE-SW with three segments namely, West (A), Centre (B) and East (C) (Kamesh Raju *et al.*, 2004). Eastern-most segment (C) has smooth bathymetry due to sediment transported and deposited by the Irrawaddy River, and has 12-15 km wide, 500m deep rift valley. Central segment (B) has partly smooth and partly rugged topography while the rugged topography and shallow valley floor devoid of sediment cover is characterized by western segment (A). A 12 km offset separates the sediment filled C segment from B segment and a ~5-6 km offset is observed between central and western segments. The spreading axis is connected by the Sagaing fault in the north and Semengko fault in the south. Based on the configuration of spreading centre and associated magnetic anomalies in the region, spreading direction during the current phase is inferred to be NW-SE (Kamesh Raju *et al.*, 2004). Alcock and Sewell seamounts are called as rise (Sheth *et al.*, 2009), are on north and south either side of the rift valley respectively

(Figure 1). It is suggested that these seamounts were together before spreading began in the Andaman Basin region (Figure. 1). Besides these two prominent seamounts, a chain of seamounts with heights varying from 500 m to 800 m are present mostly on the flanks of the rift valley.

3. Sampling Techniques And Analytical Procedures

The studied samples from Andaman backarc were collected during the first exploratory cruise MV AA Sidorenko-11. Dredging was carried out at 5 different locations, selected on the basis of morphology and tectonic setting (Table 1). Within the axial valley of the back-arc spreading centre dredging was confined to the five locations along the western segment (A).

Thin sections of representative rock samples from various tectonic features were studied for petrographical characterization. To determine geochemical composition, rocks were finely powdered (<100 micron) and fused beads were prepared for the major element analyses. Major elements were analysed by X-ray fluorescence spectrometer (XRF; Philips MAGIX PRO Model 2440) with JB-2 and BHVO-1 certified reference standards from Geological Survey of Japan and United States Geological Survey. Fused beads were prepared using Merck's Spectromelt A12 flux mixing with the finely powdered rock, heated in a platinum crucible to ~1100⁰C using conducting furnace (Minifuse2 of PANalytical). For all major elements, accuracy and precision were better than 5% RSD. Trace and rare earth element content of rocks was obtained by using the Inductively Coupled Plasma Mass Spectrometry (ICP-MS; Perkin Elmer SCIEX ELAN DRC II) at CSIR-National Geophysical Research Institute, Hyderabad, India. A mixture of doubly distilled acids (HF: HNO₃:HClO₄) mixed in the ratio 7:3:1 was used for sample open digestion. 5ml of 1ppm ¹⁰³Rh (internal standard) was added to each sample for standardization. The details regarding the instrumental parameters are given in Balaram, 1992 and Balaram and Gnaneshwar Rao, 2003. Repeated analyses of in-house standards were carried out to constrain the analytical precision and accuracy. For ICP-MS analyses, international standards JB-2 and BHVO-1 from Geological Survey of Japan and United States Geological Survey were used as certified reference materials and the accuracy and precision were found to be better than 8% RSD for all trace elements.

4. Petrography

Basalts occurring within the rift valley are megascopically vesicular, melanocratic and are fine grained to glassy in nature with thin Fe-Mn coating (Table 1). Microscopic observations suggest that these basalts are characterized by porphyritic nature with plagioclase and clinopyroxene representing phenocrystal and groundmass compositions and olivine solely occurring as phenocrysts (Table 1). Plagioclase (20-25 vol %) (Figure 2A) and olivine (Figure 2B) (~10 vol %) occur as dominant

phenocrystal phases floating on a ground mass of plagioclase microlites, clinopyroxene granules and volcanic glass (Figure 2A). In some places, plagioclase phenocrysts are clustered with each other and floats in the ground mass of plagioclase microlites, finer clinopyroxene and volcanic glass depicting glomero-porphyritic texture (Figure 2C). Compositionally, these phenocrystal plagioclase grains are showing a bytownite-labradorite [An_{69-62} determined by symmetrical extinction angle ($X^{\wedge}C$)] variety. Megacrysts of plagioclase (~3-4 mm) sometimes show zoning (Figure 2D) and contain melt inclusions. Olivine phenocrysts in basalts occasionally contain glass inclusions parallel to crystal boundaries indicating the entrapment of glass during the growth of the olivine crystal. Some of the plagioclase crystals are showing a sub ophitic nature (Figure 2E). Few basalt samples from the rift valley show minor alteration of olivine to palagonite bordering the rims of vesicles. In the groundmass, the plagioclase microlites are forming a triangular interspace which is filled up by clinopyroxene and volcanic glass depicting intergranular and intersertal texture respectively. In few places, microlites are showing the orientation of primary flow depicting a flow texture (Figure 2F).

5. Geochemistry

5.1 Major elements

The studied volcanic rocks from Andaman subduction zone have been classified on the basis of their total alkali ($Na_2O + K_2O$) vs. silica (SiO_2) variations. The studied samples plot in the fields for basalt, basaltic andesite and on the boundary demarcating the fields of basalts and trachybasalts in total alkali vs. silica (TAS) diagram (Le Bas *et al.*, 1986, Figure 3A) thereby reflecting sub alkaline compositions on AFM plot (Figure 3B). Major element chemistry (Table 2) of the studied basalts, basaltic andesites and trachybasalts are marked by moderate to high contents of SiO_2 ranging from 45.8-55.7 wt. % and Al_2O_3 varying between 13.2 and 19.1 wt. % with low to moderate concentrations of Fe_2O_3 and FeO varying in the range from 1.85-3.43 wt.% and 5.6-8.4 wt.% respectively. CaO (7.1-12.5 wt. %) and MgO (4.3-9.1 wt. %) show moderate concentrations with low MnO (0.14-0.22 wt. %), P_2O_5 (0.06-0.15 wt. %) contents. TiO_2 compositions widely range from 0.1 to 1.9 wt. %. The total alkali contents ($Na_2O + K_2O$) for these rocks ranging from 2.6 to 5.05 wt. % are consistent with mildly alkaline affinity. Geochemical parameters used for constraining the extent of magmatic differentiation like Mg# shows a wide range of variation from 29 to 51 which indicates much evolved nature of the volcanic rocks. Negative correlations of major elements like SiO_2 , Fe_2O_3 and total alkali ($Na_2O + K_2O$) with MgO are concomitant to differentiation of precursor magma controlled by crystallization of olivine, pyroxene and plagioclase. Positive variation trend for CaO with respect to MgO further corroborates accumulation of phenocrystal Ca-plagioclase during early stage of crystallization.

5.2 Trace and Rare earth elements

The studied volcanic rocks commensurately display overall depleted abundances for transitional trace elements (Ni, Cr and Co), Large Ion Lithophile Elements (LILE; Rb, Ba, Sr) and High Field Strength Elements (HFSE; Nb, Ta; Table 2) in comparison with OIB (Rb: 31 ppm, Sr: 660 ppm; Ba: 350 ppm, Nb: 48 ppm, Ta: 2.7 ppm) and primitive mantle compositions (Ni: >400 ppm, Cr: >800 ppm). These basalts show overall flat, MORB-type chondrite normalized REE patterns (Figure 4) except uniform positive chondrite-normalized Nd anomalies and negative La anomalies depicted by three samples. REE chemistry (Table 2) is characterized by (i) variable La abundances (1.02-6.2 ppm) with depleted to enriched LREE over MREE [(La/Sm)_N: 0.3-1.93] and (ii) moderate extent of MREE/HREE fractionation [(Gd/Yb)_N= 1.14-1.5, (Dy/Yb)_N= 0.95-1.05]. Primitive mantle normalized incompatible trace element patterns (Figure 4) collectively reflect uniform positive anomalies at Ba and negative Nb anomalies. Sr shows both positive and negative anomalies with respect to primitive mantle composition (Figure 4).

6. Discussion

6.1 Tectonic Setting

High field strength elements (HFSE, such as, Nb, Ta, Y) serve as reliable geochemical proxies to constrain the tectonic environments associated with magmatism in oceanic and continental realms. REE and HFSE are least sensitive to alteration and their ratios have been successfully applied to distinguish different geodynamic conditions involved in the process of magmatism (Condie, 2001, 2000; Song *et al.*, 2008; He *et al.*, 2010). In terms of Ti/Y vs. Nb/Y relationships, the studied samples with tholeiitic sub-alkaline affinity correspond to a mid-oceanic ridge setting, while a lone plot fall in the volcanic arc field (Figure 5A). On FeO^{*}/MgO vs. TiO₂ plot (Figure 5B) the basalts straddle the fields of volcanic arc front and back arc. Majority of the studied basalts occupy the compositional array for MORB, slab-distal BABB (back-arc basin basalts) and FAB (fore-arc basalts) on V vs Ti tectonic discrimination diagram (Figure 5C), while few samples correspond to the field for IAT also including slab-proximal BABB and FAB. Ti, Sc, V and Zr discrimination diagrams have been used by previous workers (Gamble *et al.*, 1994; Polat *et al.*, 1999; Manikyamba *et al.*, 2015a) to discriminate between arc, back-arc and MOR basalts. The studied samples indicate their intraoceanic back arc affinity by occupying the field of back-arc basin basalts (BABB) on Ti/Sc, Ti/V, Ti/Zr vs. Zr plots (Figure 6) implicating a gradual geodynamic transition from back arc rifting to back arc extension during the episodes of magma genesis and eruption.

6.2 Mantle processes and Magma genesis: Subduction input in back-arc mantle

Trace element geochemistry of mantle-derived magmas can be used to characterize the mantle sources and field valuable information about the nature of mantle source from which they derived. HFSE and REE, being resistant to alteration, can be successfully used to distinguish different possible melt sources and mantle-borne characters of magmas originating from diverse tectonic settings (Erlank and Kable, 1976; Pearce and Norry, 1979; Le Roex *et al.*, 1983; Ray *et al.*, 2013). The enrichment-depletion characters of the mantle source for the studied basalts have been assessed in terms of LILE/HFSE, LILE/LREE and HFSE/HFSE ratios (Pearce and Parkinson, 1993; Pearce, 2008).

The genesis and evolution of BAB magmas are primarily influenced by (i) the composition and contribution from the mantle flowing into the back-arc region (ii) influx of subduction component (iii) interaction between the MORB-type back arc mantle and arc-type, subduction-processed mantle components (iv) melt generation by partial melting of hydrous mantle ensued by assimilation/crystallization the resulting hydrous magma (Pearce and Stern, 2006; Bezos *et al.*, 2009). The arguments concerning the petrogenesis and geochemical signatures of BABB revolve around (i) extent of conditioning of depleted, MORB-type back-arc mantle by inflowing subduction components (ii) relative abundances of fluid-mobile and fluid-immobile elements and (ii) fluid control on partial melting. Back-arc basin basalts (BABBs) are generated by decompression melting and erupt along spreading centres in a manner almost indistinguishable from that of N-MORB, albeit with a mild hydrous and incompatible element enrichment (Gribble *et al.*, 1996; Smith *et al.*, 2001; Langmuir *et al.*, 2006; Manikyambaet *et al.*, 2009). Geochemical differences between the two have been established from recent paired arcs and back-arcs of the SW Pacific, where back-arc basin basalts plot on variation diagrams between Primitive Island arc basalts (IAB) and N-MORB (Woodhead and Johnson, 1993; Gamble *et al.*, 1994). The geochemical characteristics of BABBs are either transitional between MORB and arc magmas or indistinguishable from arc-derived melts due to spatial relation between arc and back-arc systems. In general, the arc basalts are characterized by LILE enrichments and HFSE depletions, while BABB are compositionally analogous to MORB-like melts with negligible LILE enrichment and HFSE depletion (Manikyambaet *et al.*, 2015a; 2015b). This typical character of BABB is maintained in mature back-arc system where the domain of back-arc basin melts is spatially separated and distinguishable from subduction-arc regime (Stern *et al.*, 1990). However, in nascent or initial back-arc rift system, the proximity between subduction-processed arc environment and back-arc basin, and the interaction between MORB-like and arc-like mantle components account for the arc-like composition of BABB. Decompressional partial melting of

asthenospheric mantle occurs under back-arc spreading centres and the residual depleted peridotitic asthenosphere is drawn by induced convection into the arc wedge. In the wedge, depleted peridotite melts under more hydrous conditions imparting higher LILE/LREE and HFSE/REE ratios relative to the back-arc due to the more refractory mantle wedge, coupled with hydrous fluxing of non-conservative elements from the slab (Woodhead *et al.*, 1993; Gamble *et al.*, 1994; Pearce and Peate, 1995; Manikyamba *et al.*, 2015a).

The studied samples show variable Nb (0.8-4.4 ppm) and Zr (46.7-106.4 ppm) contents with respect to N-MORB (Nb=2.33 ppm, Zr =74 ppm) implying their generation from an enriched to depleted mantle source (Sun and McDonough, 1989). Erlank and Kable (1976), Pearce and Norry (1979) and Le Roex *et al.* (1983) have emphasized the importance of Zr/Nb ratio as indicator of the 'depleted' or 'enriched' nature of the source region for basaltic magmas. The Zr/Nb ratios of the investigated samples range from 22.2-98.9 showing lower values in comparison to N-MORB (Zr/Nb: >301). This feature suggests that the parental melts for the studied rocks were derived through partial melting of a depleted mantle enriched by subduction processes. Zr/Ba ratio can be considered as an effective parameter to distinguish lithospheric sources (Zr/Ba: 0.3-0.5) from asthenospheric sources of parent melt (Zr/Ba: >0.5) (Menzies *et al.*, 1991; Greenough *et al.*, 1998; Kürkcüoğlu, 2010; Saha *et al.*, 2017). In the present scenario, the Zr/Ba ratio of the studied samples ranging from 0.6 to 3.02 indicates involvement of depleted asthenospheric mantle source of MORB affinity in the melting process. The LILE and compatible transitional trace element compositions for these rocks are depleted in comparison with primitive mantle and OIB that conform to a mantle depletion trend. Primitive mantle-normalized incompatible trace element and chondrite normalized REE patterns for the studied Andaman BABB (Figure 4) exhibit depleted abundances for LILE, HFSE and REE that are suggestive of generation of parent magma from a MORB-type depleted mantle source which had experienced sufficient melt extraction episodes. On TiO₂/Yb vs. Nb/Yb plot (Figure 7A), the studied samples distinctly reflect a tholeiitic N-MORB composition. However, Nb/La vs. Ba/Rb variations (Figure 7B) invoke incorporation of subduction components into MORB-type back-arc mantle for the generation of melts parental to the studied volcanic rocks. The plots for the studied samples on FeO*/MgO vs. TiO₂ and Mg# vs. SiO₂/Al₂O₃ diagrams (Figures 7C and 7D) suggest clinopyroxene crystallization and accumulations of Fe-Ti oxides in these basalts. Major element variations for the Andaman BABB are conforming to crystallization of olivine, clinopyroxene and Ca-plagioclase from a precursor melt having tholeiitic compositions. Primitive mantle normalized positive anomalies at Ba and Sr suggest plagioclase accumulation, while chondrite-normalized Nd positive anomalies attribute to pyroxene crystallization. Negative Nb anomalies commensurate with residual amphibole

in the source. Nb/Yb serves as a proxy for mantle fertility and also degree of mantle melting across arc-back arc regime (Pearce and Stern, 2006). Nb/Yb ratios for the Andaman BABB varying between 0.4-1.23 in comparison with Nb/Yb (0.4-0.8) for depleted mantle and for average N-MORB (0.8-1.6; Pearce and Stern, 2006) thereby attest to gradually decreasing influence of subduction input in the mantle from back arc rifting to back arc spreading. This geochemical feature is correlatable with higher degrees of partial melting and mantle depletion through episodic melt extraction towards volcanic arc front (Fretzdorff *et al.*, 2006). In terms of Dy/Dy^* vs. Dy/Yb variations (Figure 8A), the BABB basalts from Andaman show a MORB affinity of precursor magmas with amphibole/clinopyroxene fractionation. Chondrite-normalized REE patterns with LREE/HREE and LREE/MREE ratios (Table 2) suggest feeble to moderate LREE/HREE and LREE/MREE fractionations. This geochemical feature corroborates gradual transition from hydrous mantle melting maintained by subduction flux during initial back arc rifting to anhydrous melting of MORB-type mantle at back-arc spreading stage.

The studies on the Phanerozoic island arc systems provide significant understanding about the magmatic and tectonic processes operative in subduction zones. The mantle wedge above a subduction zone in modern arc systems have been chemically modified and enriched by components from the subducting oceanic lithosphere including (i) fluid flux derived from dehydration of altered oceanic crust or subducted sediments (ii) addition of melts of subducted slab sediments and basaltic crust (McCulloch and Gamble, 1991; Yogodzinski *et al.*, 1995; Tatsumi, 2005; Kimura and Yoshida, 2006; Zhao and Zhou, 2006; Manikyamba *et al.*, 2017). Metasomatism and flux-controlled partial melting of mantle wedge peridotites triggered by the subduction-derived components including hydrous fluids, siliceous slab melts and sediments from subducted oceanic lithosphere are widely accepted as fundamental processes for subduction zone magmatism in intraoceanic and continental arc regime (Kimura and Yoshida, 2006; van Keken *et al.*, 2011; Mullen and McCullum, 2014). As a consequence relative elemental abundances in arc magmas and across-arc compositional variations largely replicate the sub-arc mantle heterogeneity. Incompatible trace elements having similar compatibility during mantle melting like LILE, LREE and HFSE show diverse compositions in subduction-derived volcanic rocks. The characteristic enrichment in LILE-LREE enrichment with relative HFSE depletion in arc magmas reflect a selective mobility of incompatible trace elements during subduction processes or presence of HFSE-rich minerals in the system (Munker *et al.*, 2004; Manikyamba *et al.*, 2015 a, b, c; Saha *et al.*, 2018). La/Sm vs. Nb/Zr variations (Figure 8B) with chondrite-normalized positive Nd anomalies, primitive mantle normalized positive Ba anomalies, elevated abundances of Sr and selective enrichment in La over MREE imply contributions from a

mantle fluxed by fluids and sediments released and transported from a subducting oceanic slab into the back-arc mantle. The high alumina concentrations for the studied basalts (Al_2O_3 :13.2 and 19.1 wt. %) suggest high water contents in the magma source attributing to dehydration of subducted oceanic crust and fluid-transport. These geochemical observations collectively suggest chemical heterogeneity in the mantle source marked by variable contributions from a subducting oceanic crust and transitional enrichment-depletion process during rifting and spreading stages of back-arc basin development. Geochemical signatures of modern subduction zone magmas suggest influx of fluid and juvenile crustal components by subducted slab, subducted sediments and mantle wedge through either dehydration or melting are principal contributors to subduction zone magmatism (Clift *et al.*, 2005; Shuto *et al.*, 2013; Sato *et al.*, 2013; Manikyamba *et al.*, 2015b).

The subduction-derived components (fluids, melts, sediments) serve as viable agents for transfer of different elements from slab to mantle wedge. HFSEs are fluid-immobile in nature and behave as “conservative” elements during geochemical at the slab-mantle wedge interface at a particular pressure-temperature regime during the initial to intermediate stages of subduction. In contrast, LILE and LREE are fluid-mobile, “nonconservative” elements relative to HFSE and are mobilised by slab-dehydrated fluids (Munker *et al.*, 2004; Mullen and McCullum, 2013). However experimental studies advocated that the mobility of HFSE increases with rising pressure at mature subduction stages and solute contents of fluids that invoke melting of subducting slab containing residual amphibole or titanate phase like rutile. Garnet amphibolite or rutile-bearing eclogite present in deep subducting slab sources comprise phases that cause selective HFSE entrapment, restrain mobility of HFSE and control HFSE depletion in arc magma sources (Munker *et al.*, 2004; Tiepolo *et al.*, 2011; Jacques *et al.*, 2013). LILE/LREE and LILE/HFSE provide significant constraints to assess relative contributions from subduction components that account for distinct geochemical signatures in arc and back-arc magmas (Elliott *et al.*, 1997; Elburg *et al.*, 2002; Polat and Kerrich, 2006; Li *et al.*, 2013; Shuto *et al.*, 2013; Sato *et al.*, 2013; Kimura and Nakajima, 2014). Subduction-derived fluids are enriched in Ba, Pb, Rb, U and Sr and depleted in Th, Nb, Ta, Hf, Ti and REE. The LILE (Ba: 28-94 ppm, Sr: 144-339 ppm), HFSE (Nb:0.8-4.4 ppm, Zr: 46.7-108.6 ppm, Y: 13.2-34.5 ppm) and REE (La: 1.02-6.3 ppm, Ce: 8.40-16.7 ppm, Nd: 8.05-13.33 ppm, Sm: 1.76-3.74 ppm) concentrations for the Andaman BABB reflect an overall enrichment with respect to average compositions of typical N-MORB (Ba: 12ppm, Sr: 124 ppm, Nb: 3.1 ppm, Zr: 85 ppm, Y: 29 ppm, La: 3 ppm, Ce: 9 ppm, Nd: 7.7 ppm, Sm: 2.8 ppm) and are consistent with that of back-arc tholeiites (BAT; Ba: 77 ppm, Sr: 212 ppm, Nb: 8 ppm, Zr: 130 ppm, Y: 30 ppm, La: 7.83 ppm, Ce: 19 ppm, Nd: 13.1, Sm: 3.94 ppm). The subduction-influenced geochemical traits are inherited during initial

back-arc rifting from an arc-proximal mantle source fluxed with subduction-derived fluids and sediments that gradually recede with progressive back arc spreading distal from the arc. The studied volcanic rocks with Ce/Nb ranging from 3.3 to 12.7 and consistently depleted values for Nb/Y, Nb/Zr and Nb/La reflect subduction signatures in depleted MORB type mantle (DMM) and variable contributions from subduction-derived components (SDC) in their genesis (Safonova, 2009; Saunders *et al.*, 1988; Safonova *et al.*, 2008). LILE and LREE concentrations of subduction zone magmas are primarily attributed to input from slab-dehydrated fluids and sediments respectively (Plank and Langmuir, 1998). Ba/La and $(La/Sm)_N$ values increase with addition of subduction components to the magma source, while the fluid-immobile slab-conservative elements like Nb and Yb show restricted abundances (Elliott *et al.*, 1997; Elburg *et al.*, 2002; Zhao *et al.*, 2016). Geochemical signatures of modern arc-related magmatism suggest that Ba/Nb ratio is an effective geochemical proxy indicating the fluid/water content in the mantle source, while Ba/La can be used as a tracer for the total slab-derived input into the mantle wedge (Cervantes and Wallace, 2003; Yang *et al.*, 2014). Ba/Nb ratios are independent of mantle source, partial melting and fractional crystallization processes and therefore serve as reliable indicators of deep and shallow subduction inputs (Pearce and Stern, 2006). Ba/Nb ratios ranging from 12.1-81.7 in the studied basalts substantiate variable magnitudes of shallow subduction input and presence of hydrous minerals (e.g. phlogopite or amphibole) in the source region (Carr *et al.*, 1990; Patino *et al.*, 2000; Jenner *et al.*, 2009). Their Ba/La (10.14-53.2) ratios with pronounced Ba enrichment attest to input from slab-dehydrated fluids. Elevated abundances of Ba, Nd, Sr, selective enrichment in La with high Ba/La and Ba/Nb ratios for the studied basalts from Andaman back-arc suggest variable contributions from both subducted slab sediments and aqueous fluids released by slab dehydration. Therefore, the subduction signatures in these rocks reflect a combination both fluids and sediment input. Variation trends for the studied basalts on Yb/Sm vs. La/Sm (Figure 9A) and Eu/Yb vs. Ce/Yb (Figure 9B) are augmenting subduction overprints in the mantle. Plots of studied basalts on Ba/La vs. $(La/Sm)_N$ diagram (Figure 9C), suggest mixing between MORB and subduction components. The trace and REE variations in these basalts conform to gradually diminishing contributions from subduction-derived components from initial rifting to matured extensional stages of Andaman back-arc system.

6.3 Mantle melting conditions

Trace element compositions are effective tracers to decipher the mantle source characteristics, degree and depth of partial melting, open and close system magmatic processes like crustal assimilation and fractional crystallization (Lassiter *et al.*, 1995; Aldanmaz *et al.*, 2000; Condie, 2003; Reichow *et al.*, 2005; Shellnut *et al.*, 2014). Rare earth element compositions are sensitive to partial melting and

are particularly useful for understanding the mantle melting condition because their relative abundances are strongly dependent on degree of partial melting and the nature of aluminous phase (spinel or garnet) in the mantle source (Lassiter *et al.*, 1995; Reichowet *et al.*, 2005 and He *et al.*, 2010). The higher distribution coefficient of HREE (Yb) and Y for garnet account for their dominant control over the degree and depth of mantle melting (Song *et al.*, 2006). However La, Sm and Gd are incompatible and have low garnet/melt partition coefficient (Rollinson, 1993). La/Yb is strongly fractionated when melting occurs in the garnet stability field and slightly fractionated during melting in the spinel lherzolite domain (Yaxley, 2000; Xu *et al.*, 2005; Lai *et al.*, 2012). The La/Sm ratio gives a measure of LREE/HREE fractionation and is particularly sensitive to the amount of garnet left in the restite which in turn reflects the degree of melting of a garnet lherzolite source (Condie, 2001). The studied samples have $(La/Yb)_N$ ratios that attest to moderate LREE enrichment over HREE implicating high degree melting in a mantle regime having spinel peridotite composition. On Sm/Yb vs. Sm plot (Figure 10A) the studied samples cluster on the melting curve for spinel lherzolite indicating > 10 % melting, while two plots reflect ~30% melting of lherzolitic mantle transitional between spinel-garnet facies. This conjecture indicates that the melting domain extended over a variable mantle depth with occurrence of spinel and garnet as stable phase in the mantle restite. The $(La/Sm)_N$ ratios for the studied samples range from 0.3-1.93 corroborating both LREE enrichment and depletion over MREE and are in compliance with variable degrees of mantle melting. Partial melting occurring at a sufficient depth for garnet to remain in the source area will elevate the middle to heavy REE ratio (i.e. Dy/Yb, Gd/Yb) in the melt (Lassiter and DePaolo, 1997). Dy/Yb and Gd/Yb are strongly fractionated when melting occurs in the garnet stability field and nearly unfractionated during melting in the spinel peridotite domain (Yaxley, 2000; Xu *et al.*, 2005; He *et al.*, 2010; Davidson *et al.*, 2013). These attributes have made Dy/Yb and Gd/Yb distinct geochemical indicators of the presence of residual garnet during partial melting and for distinguishing melting between the spinel and garnet stability fields of lherzolitic mantle (Kelemen, 1990; Lassiter *et al.*, 1995; Condie, 2001; Duggen *et al.*, 2005; Jiang *et al.*, 2009; Yang *et al.*, 2014). $(Gd/Yb)_N$ for the studied samples [$(Gd/Yb)_N$:1.1-1.5] provides evidence for parent magma generation at mantle depths < 90 km within the stability field of spinel (Herzberg, 1992) and corroborates the involvement of spinel lherzolite mantle in the melting and generation of parent magma. High Dy/Yb ratios (>2.5) are ascribed to partial melting in the garnet stability field, while Dy/Yb ratios <1.5 are derived through melting in the stability field of spinel (Yang *et al.*, 2014). The studied volcanic rocks are characterized by Dy/Yb ratios ranging from 0.95-1.1 implying that the mantle source carried signatures of spinel lherzolite and the parental melts were generated by high degree partial melting of spinel lherzolite corresponding to depth ranging from 30-60 km. On Dy/Yb vs. La/Yb plot (Figure

10B) the samples fall in the spinel peridotite facies domain, thereby suggesting a shallow level melting regime corresponding to spinel peridotite. Therefore, it has been envisaged the $(La/Yb)_N$, $(La/Sm)_N$, $(Gd/Yb)_N$ and Dy/Yb ratios for the studied basalts collectively suggest higher degree of partial melting in spinel peridotite domain at shallow depth leaving spinel as residual phase. Ba vs. Yb plot (Figure 10C) correlates the implications for LILE enrichment, HFSE depletion and infiltration of subduction-derived fluids in the genesis of BABB (Pearce and Stern, 2006). The studied samples follow the fractionation trends for BABB from Valu Fa Ridge and Eastern Lau Spreading Centres (ELSC) in Figure 10C. Plots of the studied samples implicate transport and infiltration of slab-dehydrated fluids from volcanic arc front during initial stage of back-arc rifting and this fluid influx induced (i) enhanced abundances of fluid-mobile Ba and relative depletion in fluid-immobile Yb and (ii) higher degree of mantle melting.

6.4 Tectono-magmatic evolution of Andaman back-arc basin

Mid-oceanic ridge and back-arc rift systems are the potential active zones providing insights into the magmatic and tectonic processes involved in juvenile oceanic crust generation at intraoceanic spreading centres. A back arc tectonic regime is transitional between open mid-oceanic ridges that are devoid of subduction inputs and volcanic arc front flushed by subduction derived components slab-dehydrated fluids, siliceous slab melts, terrigenous detritus, altered oceanic crust, marine sediments, biogenic calcareous deposits, ferromanganese oxides and oxyhydroxides (Bezous *et al.*, 2009; Zhao *et al.*, 2016). The diversity in magmas generated in extensional back-arc basins are distinct from MORB and the compositional attributes of this magmatic spectrum BABB (back arc basin basalts) series (Sinton *et al.*, 2003). Basalts from Mariana, Izu, Tonga, east Scotia, Lau, ValuFa and Manus back arc basins reveal that the chemical compositions of BABB are marked by a wide range from N-MORB to E-MORB, IAB and even OIB in some rare cases (Garcia *et al.*, 1979; Pearce *et al.*, 1994; Taylor and Martinez, 2003; Bezous *et al.*, 2009). This chemical diversity has been ascribed to distinct tectonic processes operative at oceanic arc- back arc systems. The evolution of back-arc basin basalts from Andaman Sea spreading centre are conformable with that of back-arc basalts from Izu and Mariana back arcs. The BABB of Mariana Trough represents a modern-day example where the back-arc basin basalts are compositionally marked by contributions from subduction-derived component. The tectonic evolution of an intraoceanic back arc basin is marked by juvenile back arc rifting and matured back arc spreading stages. It has been envisaged that magma genesis during the initial back-arc rifting stage is primarily controlled by hydration of depleted mantle fluid-mobile subduction components transported from adjacent subducting oceanic slab and with progressive back arc extension and spreading, the influence of subduction inputs gradually

decreases resulting into decompression melting of depleted MORB-type asthenospheric mantle (Gribble *et al.*, 1998; Sinton *et al.*, 2003). During the tectonic transition from early back-arc rifting to back-arc spreading, the compositions of back-arc lavas change from arc-type to MORB-type with reducing influence of subduction components on magma composition. In view of this, it is thus inferred that the geochemical signatures of the studied basalts from Andaman back arc basin records magma genesis during different stages of back-arc evolution in the Andaman Sea. The LILE-LREE compositions for the studied basalts conform to the geochemical characteristics of their counterparts from Izu and Tonga back-arc (Figures 11A and 11B). On Ba/Yb vs. Nb/Yb plot (Figure 11B) the studied samples fall in the fields for Izu and Mariana BABB in commensuration with influx of subduction-derived components into MOR mantle. The La-enriched and La-depleted characteristics of these basalts conform to decreasing magnitude of MORB-subduction interaction from back-arc rifting to back arc extension. A schematic tectonic model (Figure 12) shows the evolutionary stages of the Andaman back arc basin from the embryonic rifting to matured spreading stages. The studied La-enriched basalts carrying geochemical imprints of subduction components and fluid flux correspond to the initial rifting stage of the back arc basin; while their depleted counterparts conform to matured spreading stage of the back arc basin devoid of any subduction input.

7. Conclusion

The studied subalkaline-tholeiitic basalts from the Andaman back arc basin show overall depleted trace element characteristics in commensuration with N-MORB type compositions normally expected for basalts generated in matured back arc spreading centres. However, the REE compositions of these basalts marked by pronounced Ba and Nd abundances in conjunction with selective enrichment in La and Sr reflect distinct geochemical attributes that are correlatable with contributions from a subducting oceanic lithosphere. Notable enrichment in selected REE and incompatible fluid-mobile trace elements are ascribed to transport and influx of slab-dehydrated fluids into depleted back arc mantle asthenosphere from volcanic arc front during initial stage of back-arc rifting in the Andaman Sea. The studied basalts were derived by 10%-30% partial melting of spinel lherzolitic mantle at a shallow depth. These observations collectively point towards a chemically heterogeneous mantle beneath Andaman back-arc and the parental melts for the studied volcanic rocks were derived from a magma source that experienced variable interactions between depleted MORB type mantle (DMM) and subduction-derived components (SDC) during back arc rifting to back arc extension. The episodes of melt generation and magma eruption were associated with a gradual geodynamic transition from incipient back arc rifting to matured back arc spreading in the Andaman Sea. The tectono-magmatic evolution of the basalts from Andaman Sea back arc basin

is consistent with the back arc basin systems of Izu, Mariana, Tonga, East Lau Spreading Centre (ELSC) and Valu Fa ridge.

Acknowledgements

Authors are grateful to the Director, CSIR-National Institute of Oceanography for his encouragement, support and permission to publish this work. Dr. P.S. Rao is thankfully acknowledged for providing the samples from Andaman back arc which he collected during the first exploratory cruise MV AA Sidorenko-11. The authors sincerely acknowledge Dr. V. Balaram, Retired Head, Geochemistry Division, CSIR-National Geophysical Research Institute for providing trace element data. The authors acknowledge the funds from Council of Scientific and Industrial Research (CSIR) under MLP-1703 project. The authors also acknowledge GAP2175 for providing the funds for excellent microscopic facility. The authors thank the handling Associate Editor and three reviewers for their insightful suggestions which have greatly improved the quality of the manuscript. This is NIO's contribution No. XXXX.

References:

- Aldanmaz, E., Pearce, J.A., Thirlwall, M.F., Mitchell, J.G. 2000.** Petrogenetic evolution of late Cenozoic, post-collision volcanism in western Anatolia, Turkey. *Journal of Volcanological and Geothermal Research* **102**, 67–95.
- Allen, C. M. 2000.** Evolution of a post-batholith dike swarm in central coastal Queensland, Australia: arc-front to backarc?. *Lithos* **51**, 331-349.
- Balaram, V., 1992.** Effect of concomitant elements on the analyte signals in ICP-MS - A case study. In: *Proceedings of the National Seminar on Modern Trends in Analytical techniques: Applications in Chemistry*, Bhattacharaya, K.G. (ed.), Guwahati University Press **9**, 162-175.
- Balaram, V., Gnaneswar Rao, T. 2003.** Rapid determination of REEs and other trace elements in geological samples by microwave acid digestion and ICP-MS. *Atomic Spectroscopy* **24**, 206-212.
- Bézos, A., Escrig, S., Langmuir, C. H., Michael, P. J., Asimow, P. D. 2009.** Origins of chemical diversity of back-arc basin basalts: A segment-scale study of the Eastern Lau Spreading Center. *Journal of Geophysical Research: Solid Earth*, **114(B6)**, DOI: 10.1029/2008JB005924
- Brandl, P. A., Hamada, M., Arculus, R. J., Johnson, K., Marsaglia, K. M., Savov, I. P., .. Li, H. 2017.** The arc arises: The links between volcanic output, arc evolution and melt composition. *Earth and Planetary Science Letters* **461**, 73-84.
- Carr, M. J., Feigenson, M. D., Bennett, E. A. 1990.** Incompatible element and isotopic evidence for tectonic control of source mixing and melt extraction along the Central American arc. *Contributions to Mineralogy and Petrology* **105**, 369-380.
- Cervantes, P., Wallace, P. J. 2003.** Role of H₂O in subduction-zone magmatism: new insights from melt inclusions in high-Mg basalts from central Mexico. *Geology* **31**, 235-238.

- Clift, P. D., Pavlis, T., DeBari, S. M., Draut, A. E., Rioux, M., Kelemen, P. B. 2005.** Subduction erosion of the Jurassic Talkeetna-Bonanza arc and the Mesozoic accretionary tectonics of western North America. *Geology***33**, 881-884.
- Condie, K. C. 2000.** Episodic continental growth models: Afterthoughts and extensions *Tectonophysics***322**, 153–162.
- Condie, K.C. 2001.** *Mantle Plumes and Their Record in Earth History*. Cambridge University Press, London. 305pp.
- Condie, K.C. 2003.** Incompatible element ratios in oceanic basalts and komatiites: tracking deep mantle sources and continental growth rates with time. *Geochemistry, Geophysics and Geosystems***4**, 2002GC000333.
- Curray, J. R. 2005.** Tectonics and history of the Andaman Sea region. *Journal of Asian Earth Sciences***25**, 187-232.
- Davidson, J., Turner, S., Plank, T. 2013.** Dy/Dy* variations arising from mantle sources and petrogenetic processes. *Journal of Petrology***54**, 525-537.
- Diehl, T., Waldhauser, F., Cochran, J. R., KameshRaju, K. A., Seeber, L., Schaff, D., Engdahl, E. R. 2013.** Back-arc extension in the Andaman Sea: Tectonic and magmatic processes imaged by high-precision teleseismic double-difference earthquake relocation. *Journal of Geophysical Research: Solid Earth***118**, 2206-2224.
- Duggen, S., Hoernle, K., van den Bogaard, P., Garbe-Schönberg, D. 2005.** Post-collisional transition from subduction-to intraplate-type magmatism in the westernmost Mediterranean: evidence for continental-edge delamination of subcontinental lithosphere. *Journal of Petrology* **46**, 1155-1201.
- Elburg, A.M., van-Bergen, V.M., Hoogewerff, J., Foden, J., Vroon, P., Zulkarnain-Iskandar, I., Nasution-Asnawir, A. 2002.** Geochemical trends across an arc-continent collision zone; magma sources and slab-wedge transfer processes below the Pantar Strait volcanoes, Indonesia. *Geochimica et Cosmochimica Acta***66**, 2771-2789.
- Elliott, T., Plank, T., Zindler, A., White, W., Bourdon, B. 1997.** Element transport from slab to volcanic front at the Mariana arc. *Journal of Geophysical Research: Solid Earth***102**, 14991-15019.
- Erlank, A. J., Kable, E. J. D. 1976.** The significance of incompatible elements in Mid-Atlantic Ridge basalts from 45° N with particular reference to Zr/Nb. *Contributions to Mineralogy and Petrology***54**, 281-291
- Fretzdorff, S., Schwarz-Schampera, U., Gibson, H. L., Garbe-Schönberg, C. D., Hauff, F., Stoffers, P. 2006.** Hydrothermal activity and magma genesis along a propagating back-arc basin: ValuFa Ridge (southern Lau Basin). *Journal of Geophysical Research-Solid Earth*,**111**, DOI: 10.1029/2005JB003967.
- Fryer, P., Taylor, B., Langmuir, C. H., Hochstaedter, A. G. 1990.** Petrology and geochemistry of lavas from the Sumisu and Torishimabackarc rifts. *Earth and Planetary Science Letters***100**, 161-178.

- Gamble, J. A., Wright, I. C., Woodhead, J.D., McCulloch, M. T. 1994.** Arc and back arc geochemistry in the southern Kermadec Arc-Ngatoro Basin and offshore Taupo Volcanic Zone, south west Pacific. In: *Volcanism associated with extension at consuming plate margins*, Gamble J. A., Wright I. C., Woodhead, J. D., McCulloch M. T. (eds.), Geological Society of London Special Publication **81**, 193-221.
- Garcia, M. O., Liu, N. W., Muenow, D. W. 1979.** Volatiles in submarine volcanic rocks from the Mariana Island arc and trough. *Geochimica et Cosmochimica Acta* **43**, 305-312.
- Greenough, J. D., Hari, K. R., Chatterjee, A. C., Santosh, M. 1998.** Mildly alkaline basalts from Pavagadh Hill, India: Deccan flood basalts with an asthenospheric origin. *Mineralogy and Petrology* **623**, 223-245.
- Gribble, R. F., Stern, R. J., Bloomer, S. H., Stüben, D., O'Hearn, T., Newman, S. 1996.** MORB mantle and subduction components interact to generate basalts in the southern Mariana Trough back-arc basin. *Geochimica et Cosmochimica Acta* **60**, 2153-2166.
- Gribble, R. F., Stern, R. J., Newman, S., Bloomer, S. H., O'Hearn, T. 1998.** Chemical and isotopic composition of lavas from the northern Mariana Trough: Implications for magmagenesis in back-arc basins. *Journal of Petrology* **39**, 125-154.
- He, Q., Xiao, L., Balta, B., Gao, R., Chen, J. 2010.** Variety and complexity of the late Permian Emeishan basalts: reappraisal of plume-lithosphere interaction process. *Lithos* **119**, 91-107.
- Herzberg, C. 1992.** Depth and degree of melting of komatiites. *Journal of Geophysical Research* **97**, 4521-4540.
- Hofmann, A. W. 1997.** Mantle geochemistry: the message from oceanic volcanism. *Nature* **385**, 219-229.
- Inglis, E. C., Debret, B., Burton, K. W., Millet, M. A., Pons, M. L., Dale, C. W., ... Williams, H. M. 2017.** The behaviour of iron and zinc stable isotopes accompanying the subduction of mafic oceanic crust: A case study from Western Alpine Ophiolites. *Geochemistry, Geophysics, Geosystems* **18**, 2562-2579.
- Irvine, T. N. J., Baragar, W. R. A. F. 1971.** A guide to the chemical classification of the common volcanic rocks. *Canadian journal of earth sciences* **8**, 523-548.
- Jacques, G., Hoernle, K., Gill, J., Hauff, F., Wehrmann, H., Garbe-Schonberg, D., van den Boggard, P., Bindeman, I., Lara, L.E. 2013.** Across-arc geochemical variations in the Southern Volcanic Zone, Chile (34.5–38.0°S): Constraints on mantle wedge and slab input compositions. *Geochimica et Cosmochimica Acta* **123**, 218-243.
- Jenner, F. E., Bennett, V. C., Nutman, A. P., Friend, C. R., Norman, M. D., Yaxley, G. 2009.** Evidence for subduction at 3.8 Ga: geochemistry of arc-like metabasalts from the southern edge of the Isua Supracrustal Belt. *Chemical Geology* **261**, 83-98.
- Jiang, Y. H., Jiang, S. Y., Dai, B. Z., Liao, S. Y., Zhao, K. D., Ling, H. F. 2009.** Middle to late Jurassic felsic and mafic magmatism in southern Hunan province, southeast China: Implications for a continental arc to rifting. *Lithos* **107**, 185-204

- Jourdain, A., Singh, S. C., Escartin, J., Klinger, Y., KameshRaju, K. A., McArdle, J. 2016.** Crustal accretion at a sedimented spreading center in the Andaman Sea. *Geology* **44**, 351-354.
- Jung, C., Jung, S., Hoffer, E., Berndt, J., 2006.** Petrogenesis of Tertiary mafic alkaline magmas in the Hoheifel, Germany. *Journal of Petrology* **47**, 1637–1671.
- KameshRaju, K. A., Ramprasad, T., Rao, P. S., Rao, B. R., Varghese, J. 2004.** New insights into the tectonic evolution of the Andaman basin, northeast Indian Ocean. *Earth and Planetary Science Letters* **221**, 145-162.
- Kelemen, P., 1990.** Reaction between ultramafic rock and fractionating basaltic liquid I. Phase relations, the origin of calc-alkaline magma series, and the formation of discordant dunite. *Journal of Petrology* **31**, 51-98.
- Keller, N. S., Arculus, R. J., Hermann, J., Richards, S. 2008.** Submarine back-arc lava with arc signature: Fonualei Spreading Center, northeast Lau Basin, Tonga. *Journal of Geophysical Research: Solid Earth* **113**, DOI: 10.1029/2007JB005451.
- Kelley, K. A., Plank, T., Grove, T. L., Stolper, E. M., Newman, S., Hauri, E. 2006.** Mantle melting as a function of water content beneath back-arc basins. *Journal of Geophysical Research: Solid Earth* **111**, DOI: 10.1029/2005JB003732.
- Kimura, J. I., Nakajima, J. 2014.** Behaviour of subducted water and its role in magma genesis in the NE Japan arc: A combined geophysical and geochemical approach. *Geochimica et Cosmochimica Acta* **143**, 165-188.
- Kimura, J. I., Yoshida, T. 2006.** Contributions of slab fluid, mantle wedge and crust to the origin of Quaternary lavas in the NE Japan arc. *Journal of Petrology* **47**, 2185-2232.
- Kinzler, R.J., 1997.** Melting of mantle peridotite at pressures approaching the spinel to garnet transition: application to midocean ridge basalt petrogenesis. *Journal of Geophysical Research* **102**, 853-874.
- Kürkcüoğlu, B., 2010.** Geochemistry and Petrogenesis of basaltic rocks from the Develidağ volcanic complex, Central Anatolia, Turkey. *Journal of Asian Earth Sciences* **37**, 42-51.
- Lai, S., Qin, J., Li, Y., Li, S., Santosh, M. 2012.** Permian high Ti/Y basalts from the eastern part of Emeishan Large igneous province, southwestern China: petrogenesis and tectonic implications. *Journal of Asian Earth Sciences* **47**, 216-230.
- Langmuir, C. H., Bezos, A., Escrig, S., Parman, S. W. 2006.** Chemical systematics and hydrous melting of the mantle in back-arc basins. *Back-Arc Spreading Systems: Geological, Biological, Chemical, and Physical Interactions, Geophysical Monograph* **166**, 87-146.
- Lassiter, J.C., DePaolo, D.J. 1997.** Plume/lithosphere interaction in the generation of continental and oceanic flood basalts: chemical and isotopic constraints. In: *Large Igneous Provinces: continental, oceanic and planetary volcanism*, Mahoney J.J., Coffin M., (eds),. American Geophysical Union Monograph Series, 335-355.
- Lassiter, J.C., DePaolo, D.J., Mahoney, J.J. 1995.** Geochemistry of the Wrangellia Flood Basalt Province: implications for the role of continental and oceanic lithosphere in flood basalt genesis. *Journal of Petrology* **36**, 983-1009.

- Le Bas M., Maitre, R. L., Streckeisen, A., Zanettin, B. 1986.** IUGS Subcommission on the Systematics of Igneous Rocks 1986. A chemical classification of volcanic rocks based on the total alkali-silica diagram. *Journal of Petrology***27**, 745-750.
- Le Roex, A. P., Dick, H. J. B., Erlank, A. J., Reid, A. M., Frey, F. A., Hart, S. R. 1983.** Geochemistry, mineralogy and petrogenesis of lavas erupted along the Southwest Indian Ridge between the Bouvet Triple Junction and 11 degrees east. *Journal of Petrology***24**, 267-318.
- Lee, C., Wada, I. 2017.** Clustering of arc volcanoes caused by temperature perturbations in the back-arc mantle. *Nature Communications***8**, DOI: 10.1038/ncomms15753.
- Li, Y-B, Kimura, J-I., Machida, S., Ishii, T., Ishiwatari, A., Maruyama, S., Qiu, H-N., Ishikawa, T., Kato, Y., Haraguchi, S., Takahata, N., Hirahara, Y., Miyazaki, T. 2013.** High-Mg adakite and low-Carbonite from a Bonin Fore-arc seamount: implications for the reaction between slab melts and depleted mantle. *Journal of Petrology***54**, 1149-1175.
- Lodolo, E., Coren, F., Ben-Avraham, Z. 2013.** How do long-offset oceanic transforms adapt to plate motion changes? The example of the Western Pacific-Antarctic plate boundary. *Journal of Geophysical Research: Solid Earth***118**, 1195-1202.
- Manikyamba, C., Ganguly, S., Santosh, M., Subramanyam, K. S. V. 2017.** Volcano-sedimentary and metallogenic records of the Dharwar greenstone terranes, India: Window to Archean plate tectonics, continent growth, and mineral endowment. *Gondwana Research***50**, 38-66.
- Manikyamba C., Santosh M., Chandan Kumar B., Rambabu S., Li T., Saha A., Khelen A.C., Ganguly S., Singh D., Subba Rao D.V. 2016.** Zircon U-Pb geochronology, Lu-Hf isotope systematics, and geochemistry of bimodal volcanic rocks and associated granitoids from Kotri Belt, Central India: implications for Neoproterozoic-Paleoproterozoic crustal growth. *Gondwana Research***38**, 313-333.
- Manikyamba, C., Ganguly, S., Santosh, M., Saha, A., Chatterjee, A., Khelen, A. C. 2015a.** Neoproterozoic arc–juvenile back-arc magmatism in eastern Dharwar Craton, India: geochemical fingerprints from the basalts of Kadiri greenstone belt. *Precambrian Research***258**, 1-23.
- Manikyamba, C., Ganguly, S., Santosh, M., Singh, M. R., Saha, A. 2015b.** Arc-nascent back-arc signature in metabasalts from the Neoproterozoic Jonnagiri greenstone terrane, Eastern Dharwar Craton, India. *Geological Journal***50**, 651-669
- Manikyamba, C., Ray, J., Ganguly, S., Singh, M.R., Santosh, M., Saha, A., Satyanarayanan, M. 2015c.** Boninitic metavolcanic rocks and island arc tholeiites from the Older Metamorphic Group (OMG) of Singhbhum Craton, eastern India: geochemical evidence for Archean subduction processes. *Precambrian Research***271**, 138-159.
- Manikyamba, C., Kerrich, R., Khanna, T.C., Satyanarayanan, M., Krishna, A.K. 2009.** Enriched and depleted arc basalts, with high-Mg andesites and adakites: a potential paired arc-backarc of the 2.7 Ga Hutti greenstone terrane, India. *Geochimica et Cosmochimica Acta***73**, 1711-1736.
- Martinez, F., Taylor, B., 2002.** Mantle wedge control on back-arc crustal accretion. *Nature* **416**, 417-420.

- Masuda, H., Fryer, P. 2015.** Geochemical characteristics of active backarc basin volcanism at the southern end of the Mariana Trough. In: *Sub seafloor Biosphere Linked to Hydrothermal Systems*, Springer, Japan, pp. 261-273.
- McCulloch, M.T., Gamble, A.J. 1991.** Geochemical and geodynamical constraints on subduction zone magmatism. *Earth and Planetary Science Letters* **102**, 358-374.
- Menzies, M.A., Kyle, P.R., Jones, M., Ingram, G. 1991.** Enriched and depleted source components for tholeiitic and alkaline lavas from Zuni-Bandera, New Mexico: inferences about intraplate processes and stratified lithosphere. *Journal of Geophysical Research* **96**, 13645-13671.
- Mullen, E. K., McCallum, I. S. 2014.** Origin of basalts in a hot subduction setting: Petrological and geochemical insights from Mt. Baker, Northern Cascade Arc. *Journal of Petrology* **55**, 241-281.
- Munker, C., Worner, G., Yogodzinski, G., Churikova, T. 2004.** Behaviour of high field strength elements in subduction zones: constraints from Kamchatka–Aleutian arc lavas. *Earth and Planetary Science Letters* **224**, 275-293.
- Niu, Y., O'Hara, M. J. 2009.** MORB mantle hosts the missing Eu (Sr, Nb, Ta and Ti) in the continental crust: new perspectives on crustal growth, crust–mantle differentiation and chemical structure of oceanic upper mantle. *Lithos* **112**, 1-17.
- Patino, L. C., Carr, M. J., Feigenson, M. D. 2000.** Local and regional variations in Central American arc lavas controlled by variations in subducted sediment input. *Contributions to Mineralogy and Petrology* **138**, 265-283
- Pearce J.A. 1982.** Trace element characteristics of lavas from destructive plate boundaries. In: *Andesites*, Thorpe R.S. (ed.), Wiley, New York, p. 525-548.
- Pearce, J. A., Ernewein, M., Bloomer, S. H., Parson, L. M., Murton, B. J., Johnson, L. E. 1994.** Geochemistry of Lau Basin volcanic rocks: influence of ridge segmentation and arc proximity. *Geological Society of London, Special Publications* **81**, 53-75.
- Pearce, J. A., Norry, M. J. 1979.** Petrogenetic implications of Ti, Zr, Y, and Nb variations in volcanic rocks. *Contributions to Mineralogy and Petrology* **69**, 33-47.
- Pearce, J. A., Parkinson, I. J. 1993.** Trace element models for mantle melting: application to volcanic arc petrogenesis. *Geological Society of London, Special Publications* **76**, 373-403.
- Pearce, J. A., Peate, D. W. 1995.** Tectonic implications of the composition of volcanic arc magmas. *Annual Review of Earth and Planetary Sciences* **23**, 251-285
- Pearce, J.A. 2008.** Geochemical fingerprinting of oceanic basalts with applications to ophiolite classification and the search for Archean oceanic crust. *Lithos* **100**, 14-48.
- Pearce, J.A., Stern, R.J. 2006.** Origin of Back-Arc Basin Magmas: Trace Element and Isotope Perspectives. Back-Arc Spreading Systems: Geological, Biological, Chemical and Physical Interactions. *Geophysical Monograph Series* **166**, 63-86.
- Plank, T., Langmuir, C.H. 1998.** The chemical composition of subducting sediments and its consequences for the crust and mantle. *Chemical Geology* **145**, 325-394.

- Polat, A., Kerrich, R. 2006.** Reading the geochemical fingerprints of Archean hot subduction volcanic rocks: evidence for accretion and crustal recycling in a mobile tectonic regime. *American Geophysical Monograph* **164**, 189-213.
- Polat, A., Kerrich, R., Wyman, D. A. 1999.** Geochemical diversity in oceanic komatiites and basalts from the late Archean Wawa greenstone belts, Superior Province, Canada: trace element and Nd isotope evidence for a heterogeneous mantle. *Precambrian Research* **94**, 139-173.
- Rao, P. S., KameshRaju, K. A., Ramprasad, T., Nath, B. N., Rao, B. R., Rao, C. M., Nair, R. R. 1996.** Evidence for hydrothermal activity in the Andaman Backarc Basin. *Current Science* **70**, 379-385.
- Ray J., Saha A., Koeberl C., Thoni M., Ganguly S., Hazra S. 2013.** Geochemistry and Petrogenesis of Proterozoic mafic rocks from East Khasi Hills, Shillong Plateau, Northeastern India. *Precambrian Research* **230**, 119-137.
- Reichow, M. K., Saunders, A. D., White, R. V., Al'Mukhamedov, A. I., Medvedev, A. Y. 2005.** Geochemistry and petrogenesis of basalts from the West Siberian Basin: an extension of the Permo–Triassic Siberian Traps, Russia. *Lithos* **79**, 425-452.
- Rollinson, H.R. 1993.** Using geochemical data: evolution, presentation, interpretation. Longman Group UK Limited, Singapore
- Safonova, I.Yu. 2009.** Intraplate magmatism and oceanic plate stratigraphy of the Paleo-Asian and Paleo-Pacific Oceans from 600 to 140 Ma. *Ore Geology Reviews* **35**, 137-154.
- Safonova, I.Yu., Simonov, V.A., Buslov, M.M., Ota, T., Maruyama, Sh. 2008.** Neoproterozoic basalts of the Paleo-Asian Ocean (Kurai accretion zone, Gorny Altai, Russia): geochemistry, petrogenesis, geodynamics. *Russian Geology and Geophysics* **49**, 254-271.
- Saha A., Ganguly S., Ray J., Koeberl C., Thoni M., Sarbajna C., Sawant S.S. 2017.** Petrogenetic evolution of Cretaceous Samchampi-Samteran Alkaline Complex, Mikir Hills, Northeastern India: Implications on multiple melting events of heterogeneous plume and metasomatized sub-continental lithospheric mantle. *Gondwana Research* **48**, 237-256.
- Saha, A., Santosh, M., Ganguly, S., Manikyamba, C., Ray, J., Dutta, J. 2018.** Geochemical cycling during subduction initiation: Evidence from serpentinized mantle wedge peridotite in the south Andaman ophiolite suite. *Geoscience Frontiers*, <https://doi.org/10.1016/j.gsf.2017.12.017>
- Sato, M., Shuto, K., Uematsu, M., Takahashi, T., Ayabe, M., Takanashi, K., Ishimoto, H., Kawabata, H. 2013.** Origin of Late Oligocene to Middle Miocene adakitic andesites, high magnesian andesites and basalts from the back-arc margin of the SW and NE Japan arcs. *Journal of Petrology* **54**, 481-524.
- Saunders, A. D., Norry, M. J., Tarney, J. 1988.** Origin of MORB and chemically-depleted mantle reservoirs: trace element constraints. *Journal of Petrology Special Lithosphere Issue*, 415-445.
- Shellnutt, J.G., Bhat, G.M., Wang, K., Brookfield, M.E., Jahn, B., Dostal, J. 2014.** Petrogenesis of the flood basalts from the Early Permian Panjal Traps, Kashmir, India: Geochemical evidence for shallow melting of the mantle. *Lithos* **204**, 159-171.

- Shervais, J. W. 1982.** Ti-V plots and the petrogenesis of modern and ophiolitic lavas. *Earth and Planetary Science Letters***59**, 101-118.
- Sheth, H. C., Ray, J. S., Bhutani, R., Kumar, A., Smitha, R. S. 2009.** Volcanology and eruptive styles of Barren Island: An active mafic stratovolcano in the Andaman Sea, NE Indian Ocean. *Bulletin of Volcanology***71**, 1021-1039.
- Shuto, K., Sato, M., Kawabata, H., Osanai, Y., Nakano, N., Yashima, R. 2013.** Petrogenesis of Middle Miocene Primitive Basalt, Andesite and Garnet-bearing Adakitic Rhyodacite from the Ryozen Formation: Implications for the Tectono-magmatic Evolution of the NE Japan Arc. *Journal of Petrology***54**, 2413-2454.
- Sinton, J., Detrick, R., Canales, J. P., Ito, G., Behn, M. 2003.** Morphology and segmentation of the western Galápagos Spreading Center, 90.5–98 W: Plume-ridge interaction at an intermediate spreading ridge. *Geochemistry, Geophysics, Geosystems***4**
- Smith, G. P., Wiens, D. A., Fischer, K. M., Dorman, L. M., Webb, S. C., Hildebrand, J. A. 2001.** A complex pattern of mantle flow in the Lau backarc. *Science***292**, 713-716.
- Smith, W. H., Sandwell, D. T. 1997.** Global sea floor topography from satellite altimetry and ship depth soundings. *Science* **277**, 1956-1962.
- Song, X.Y., Zhou, M.F., Keays, R.R., Cao, Z.M., Sun, M., Qi, L. 2006.** Geochemistry of the Emeishan flood basalts at Yangliuping, Sichuan, SW China: implications for sulphide segregation. *Contributions to Mineralogy and Petrology***152**, 53-74.
- Song, X-Y., Qi, H-W., Robinson, P.T., Zhou, M-F., Cao, Z-M., Chen L-M. 2008.** Melting of the subcontinental lithospheric mantle by the Emeishan mantle plume; evidence from the basal alkaline basalts in Dongchuan, Yunan, Southwestern China. *Lithos***100**, 93-111.
- Stern, R.J., Lin, P-N., Morris, J.D., Jackson, M.C., Fryer, P., Bloomer, S.H., Ito, E. 1990.** Enriched back-arc basin basalts from the northern Mariana Trough: implications for the magmatic evolution of back-arc basins. *Earth and Planetary Science Letters***100**, 210-225.
- Stolper, E., Newman, S. 1994.** The role of water in the petrogenesis of Mariana trough magmas. *Earth and Planetary Science Letters***121**, 293-325.
- Sun, S.S., McDonough, W.F. 1989.** Chemical and isotopic systematics of oceanic basalts, implications for mantle composition and processes. In: *Magmatism in the Ocean Basins*, Saunders A.D., Norry M.J. (eds.), Geological Society of London Special Publication 42, UK, pp. 313-345.
- Tatsumi, Y., Eggins, S. 1995.** Subduction zone magmatism, Wiley, v. 1.
- Tatsumi, Y. 2005.** The subduction factory: how it operates in the evolving Earth. *GSA today***15**, 4.
- Taylor, B., Martinez, F. 2003.** Back-arc basin basalt systematics. *Earth and Planetary Science Letters***210**, 481-497
- Tiepolo, M., Botazzi, P., Foley, S.F., Oberti, R., Vannucci, R., Zanetti, A. 2011.** Fractionation of Nb and Ta from Zr and Hf at mantle depths: the role of titanite and kaersutite. *Journal of Petrology***42**, 221-232.

- vanKeken, P. E., Hacker, B. R., Syracuse, E. M., Abers, G. A. 2011.** Subduction factory: 4. Depth-dependent flux of H₂O from subducting slabs worldwide. *Journal of Geophysical Research: Solid Earth* **116**, DOI: 10.1029/2010JB007922
- Walter, M.J. 1998.** Melting of garnet peridotite and the origin of komatiite and depleted lithosphere. *Journal of Petrology* **39**, 29-60.
- Wiens, D. A., Kelley, K. A., Plank, T. 2006.** Mantle temperature variations beneath back-arc spreading centers inferred from seismology, petrology, and bathymetry. *Earth and Planetary Science Letters* **248**, 30-42.
- Woodhead, J.D., Johnson, R.W. 1993.** Isotopic and trace-element profiles across the New Britain island arc, Papua New Guinea. *Contributions to Mineralogy and Petrology* **113**, 479-491.
- Xu, Y-G., Ma, J-L., Frey, F.A., Feigenson, M.D., Liu, J-F. 2005.** Role of lithosphere–asthenosphere interaction in the genesis of Quaternary alkali and tholeiitic basalts from Datong, western North China Craton. *Chemical Geology* **224**, 247-271.
- Yang, Q.Y., Santosh, M., Shen, J.F., Li, S.R. 2014.** Juvenile vs. recycled crust in NE China: Zircon U–Pb geochronology, Hf isotope and an integrated model for Mesozoic gold mineralization in the Jiadong Peninsula. *Gondwana Research* **25**, 1445-1468.
- Yaxley, G., 2000.** Experimental study of the phase and melting relations of homogeneous basalt + peridotite mixtures and implications for the petrogenesis of flood basalts. *Contributions to Mineralogy and Petrology* **139**, 326-338.
- Yogodzinski, G.M., Kay, R.W., Volynets, O.N., Koloskov, A.V., Kay, S.M. 1995.** Magnesian andesite in the western Aleutian Komandorsky region: Implications for slab melting and processes in the mantle wedge. *Geological Society of America Bulletin* **107**, 505-519.
- Zhao, G., Luo, W., Lai, Z., Tian, L., Xu, C. 2016.** Influence of subduction components on magma composition in back-arc basins: a comparison between the Mariana and Okinawa troughs. *Geological Journal* **51**, 357-367.
- Zhao, J.J., Zhou, M.F. 2007.** Geochemistry of Neoproterozoic mafic intrusions in the Panzhihua district (Sichuan Province, SW China): implications for subduction related metasomatism in the upper mantle. *Precambrian Research* **152**, 27-47.

Figure Caption:

Figure 1. Map showing the location of study area along with some important tectonic features. Multibeam bathymetry from Kamesh Raju *et al.*, 2004 has been used. ABSC represents Andaman Back Arc Spreading Center, black squares denote the sampling locations along the spreading center. WAF denotes the West Andaman Fault. The background image in shades of blue is from the topo grid (Smith and Sandwell, 1997), the lighter shade represents shallow regions. The outline of Alcock and Sewell rises is denoted by white line. Inset map shows the Indian Ocean, Andaman Sea and the study area.

Figure 2. (A) Photomicrograph showing the occurrence of plagioclase, olivine (pseudomorph) and clinopyroxene phenocrysts embedded in a groundmass of plagioclase microlites, granular clinopyroxene and volcanic glass depicting porphyritic texture in backarc basalts. (B) Photomicrograph showing the occurrence of olivine phenocryst in backarc basalts. Alteration is noted along the fracture of the olivine grain. (C) Photomicrograph showing cluster of plagioclase phenocrysts floating on a hypocrySTALLINE groundmass depicting glomero-porphyritic texture in backarc basalts. (D) Photomicrograph showing oscillatory zoning in plagioclase phenocryst in backarc basalts. (E) Photomicrograph showing sub-ophitic texture marked by presence of plagioclase lath partially enclosed by clinopyroxene grain. (F) Photomicrograph showing preferential alignment of plagioclase microlites indicating a primary flow texture in backarc basalts.

Figure 3. (A) Total alkali vs. silica diagram for the Andaman backarc basalts (after LeBas *et al.*, 1986). (B) Andaman backarc basalts showing a tholeiitic to calc-alkaline trend ($\text{Na}_2\text{O} + \text{K}_2\text{O}$) – FeO^* - MgO (AFM) diagram (after Irvine and Baragar, 1971).

Figure 4. Chondrite normalized REE patterns and primitive mantle normalized multi-element spiderdiagram for the studied basalts (normalization values are from Sun and McDonough, 1989).

Figure 5. (A) Ti/Y vs. Nb/Y discrimination plot (after Pearce, 1982) depicting sub-alkaline nature of the studied samples occupying the field of Mid Oceanic Ridge (MOR). (B) FeO^*/MgO vs. TiO_2 variation plot for Andaman back arc basalts (Field after Allen, 2000). (C) Ti vs. V diagram (after Shervias, 1982) showing plots of studied samples straddling fields of MORB and slab distal backarc basin basalts and fore arc basalts with minor spill to island arc tholeiite.

Figure 6. (A) Ti/Sc (B) Ti/V and (C) Ti/Zr vs. Zr plots (after Gribble *et al.*, 1996) indicating the back arc signatures for the studied samples

Figure 7. (A) Nb/Yb vs. TiO_2/Yb diagram showing N-MORB affinity for studied samples. (B) Plots of Andaman backarc basalts in Ba/Rb vs. Nb/La diagram reflecting the influence of subduction-derived components for generation of parent magma. (C) Plot showing clinopyroxene and Ti-magnetite fractionation in the studied basalts (Allen, 2000). (D) $\text{SiO}_2/\text{Al}_2\text{O}_3$ vs Mg# variations corroborating tholeiitic differentiation trend with Fe-Ti accumulation for Andaman backarc basalts.

Figure 8. (A) Dy/Dy^* vs. Dy/Yb plot for the studied basalts (after Davidson *et al.*, 2013) indicating amphibole/clinopyroxene fractionation during magma genesis from an LREE-depleted MORB-type mantle. (B) La/Sm vs. Nb/Zr diagram for the studied basalts justifying magma generation from a N-MORB type mantle source that experienced prior depletion by melt extraction episodes ensued by influx of subduction components (values after Sun and McDonough, 1989) (Clift *et al.*, 2005).

Figure 9. Plots of (A) Yb/Sm vs. La/Sm (B) Eu/Yb vs. Ce/Yb and (C) $(\text{La}/\text{Sm})_N$ vs. Ba/La for the studied backarc basalts.

Figure 10. (A) Plots of Sm/Yb vs. Sm(after Zhao and Zhou, 2007) for the studied samples corresponding to spinel lherzolite mantle melting. Melting curves are after Aldanmazer *et al.* (2000). A pair of melt mode curves are drawn for spinel (Kinzler, 1997) and garnet (Walter, 1998) lherzolite. (B) Dy/Yb vs. La/Yb plot for the Andaman backarc basalts indicating magma generation at shallower depth in spinel-peridotite stability field (after Jung *et al.*, 2006). (C) Diagram showing the LILE (exemplified by Ba) enrichment and fluid-controlled high degree partial melting in basalts from Andaman back arc (details are in Pearce and Stern, 2006).

Figure 11. (A) La/Sm vs. Nb/Zr plot showing geochemical affinity of Andaman back arc with their counterparts from Izu and Tonga arc systems (Clift *et al.*, 2015 and references therein). (B) Plots of studied samples falling in the fields of Mariana and Izu back arc basin basalts in Ba/Yb vs. Nb/Yb diagram (after Pearce and Stern, 2006).

Figure 12. Schematic model showing basaltic magmatism in Andaman arc-backarc system. Stage I corresponds to initial opening and rifting stage of a juvenile back arc, while Stage II represents matured spreading stage of Andaman back arc evolution.

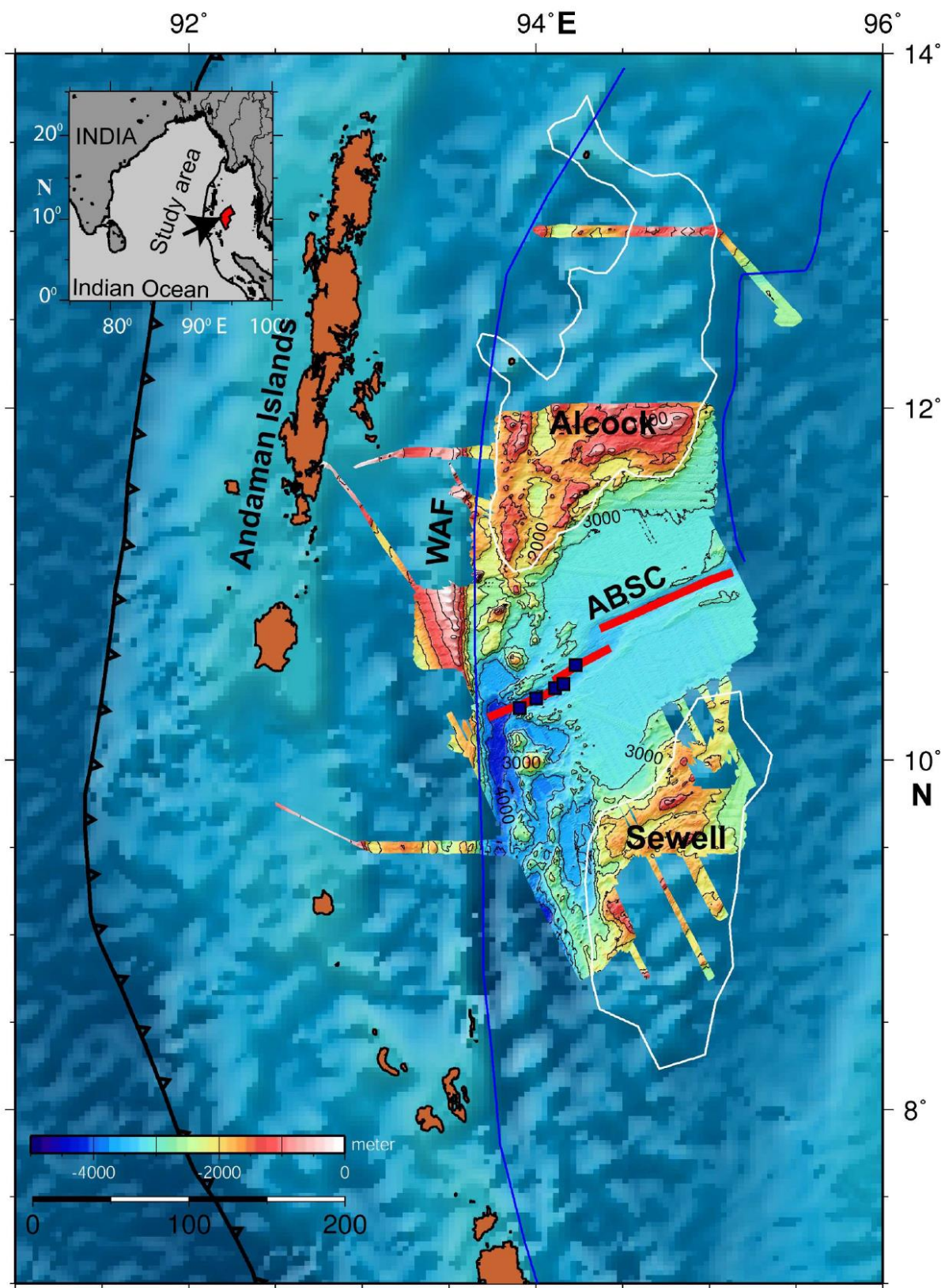


Fig.1

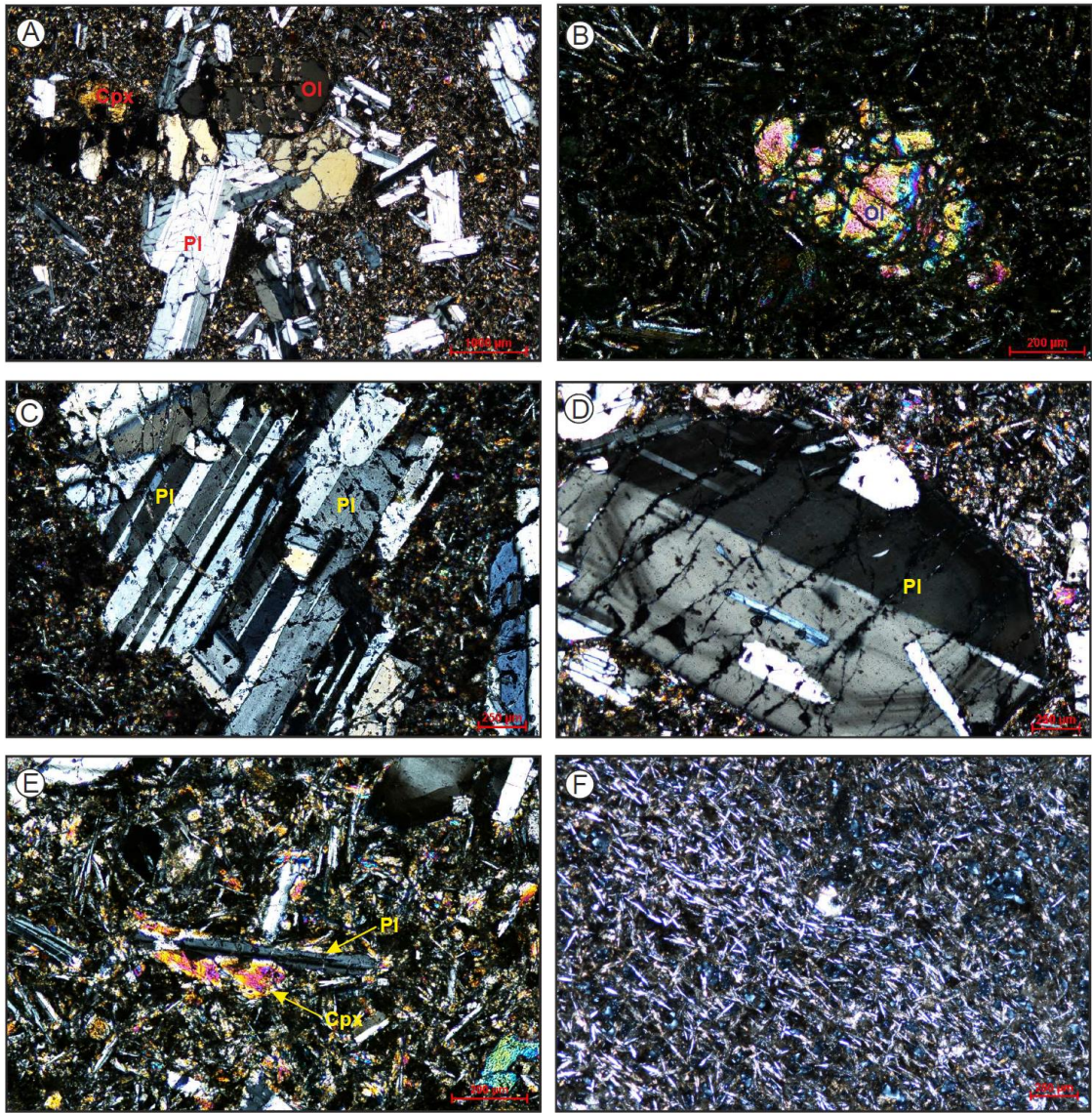


Fig.2

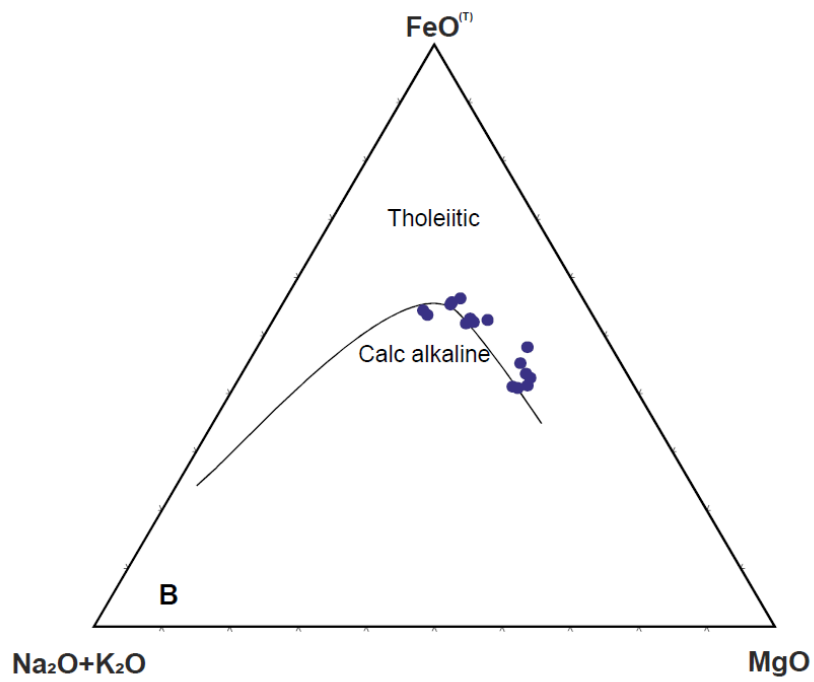
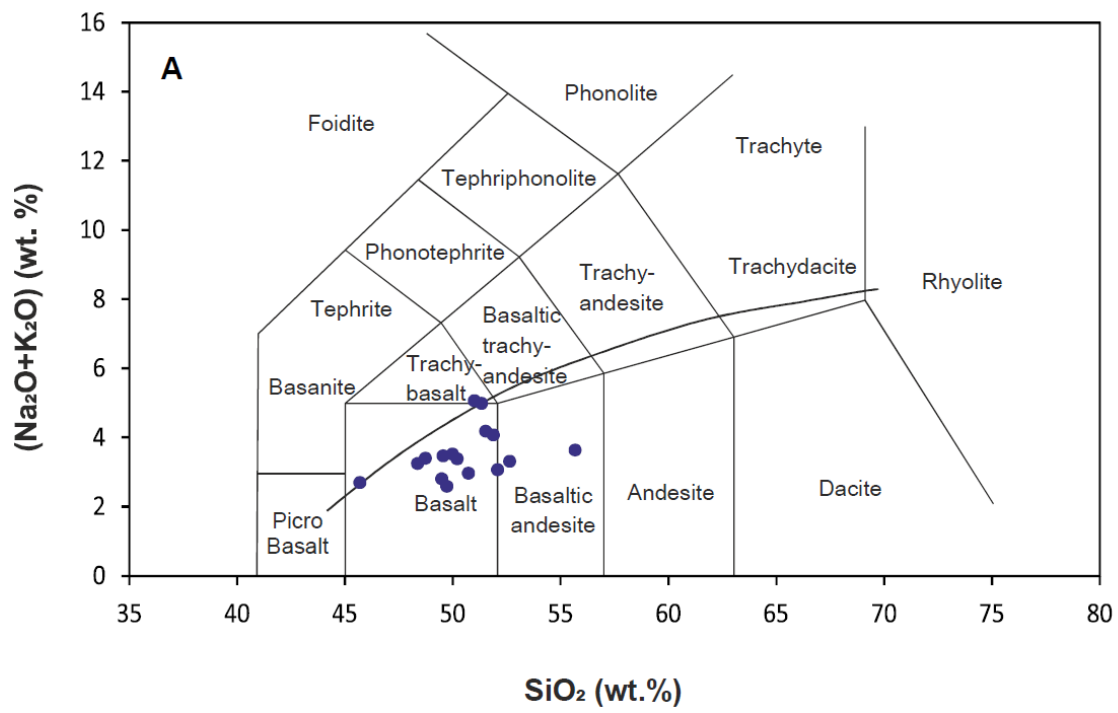


Fig.3

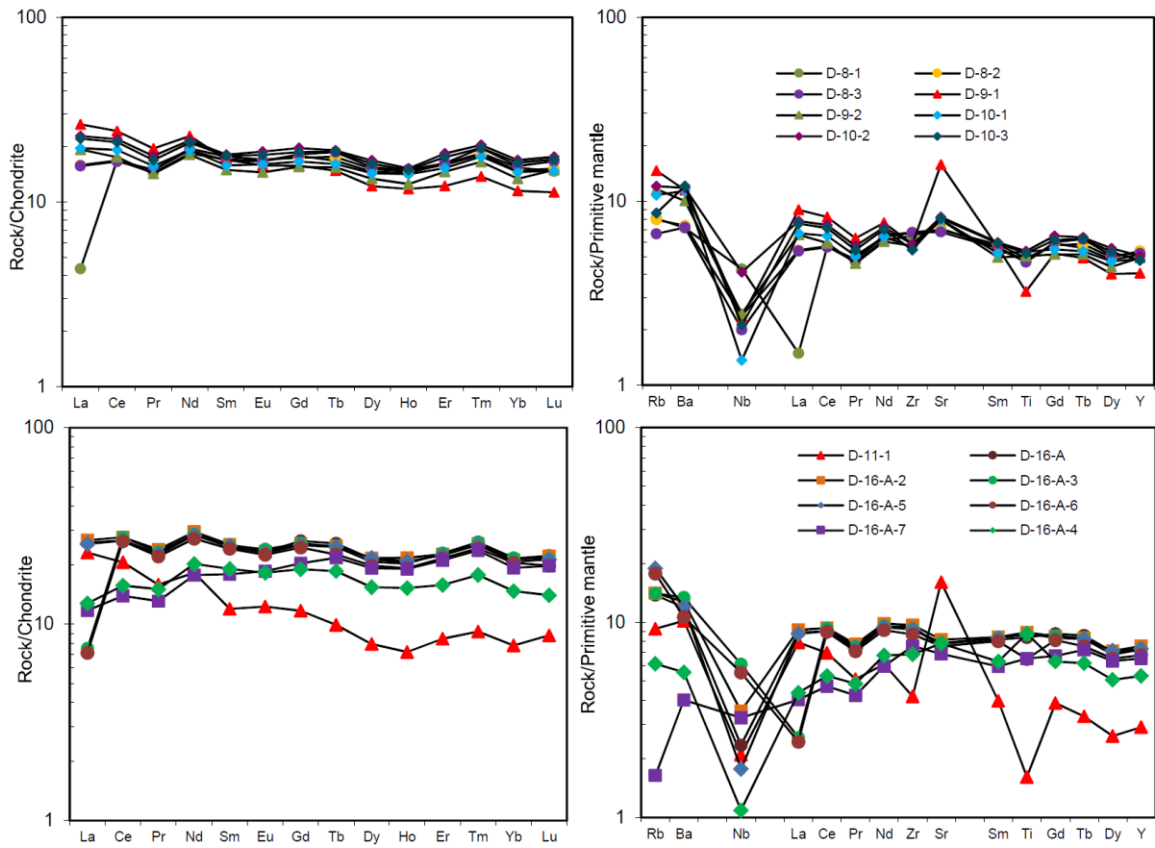


Fig. 4

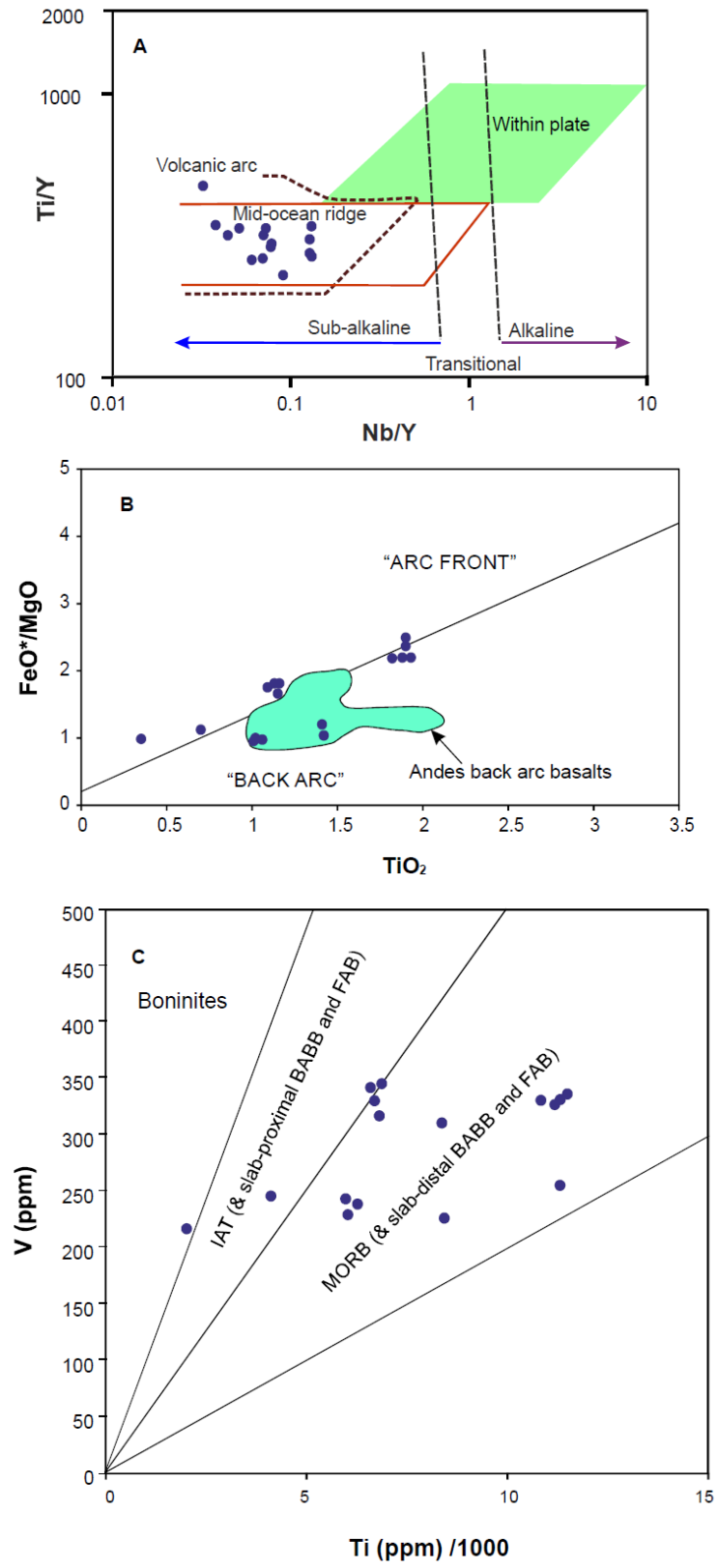


Fig.5

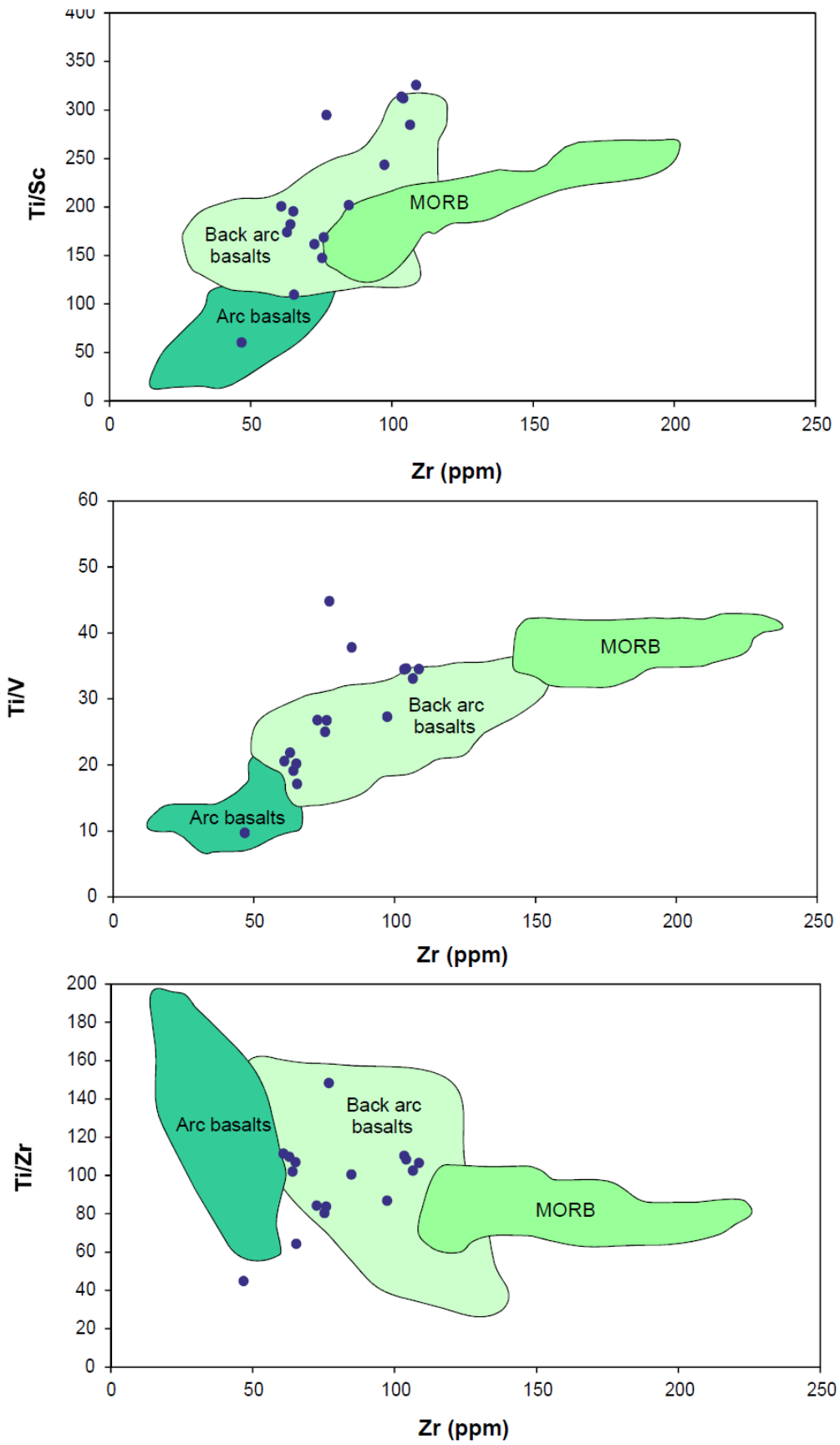


Fig :6

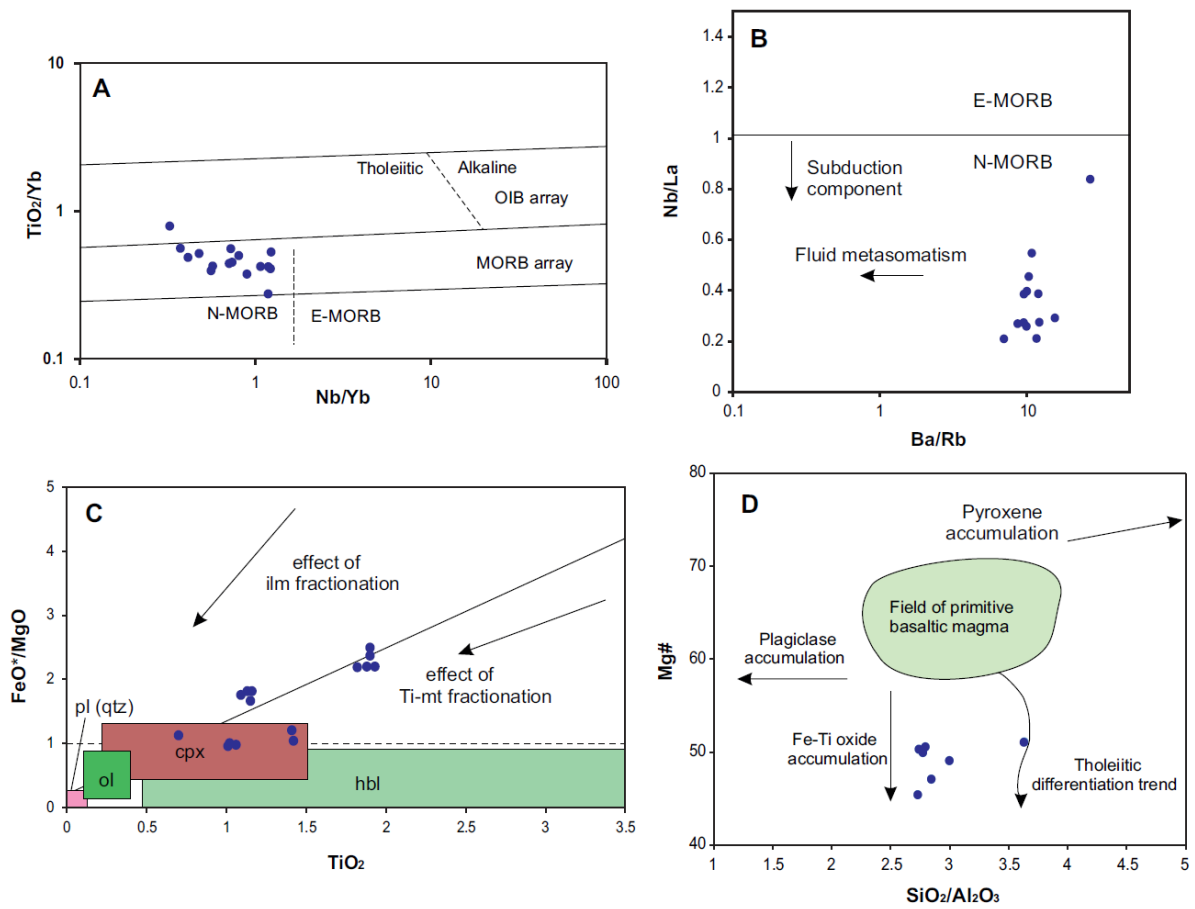


Fig.7

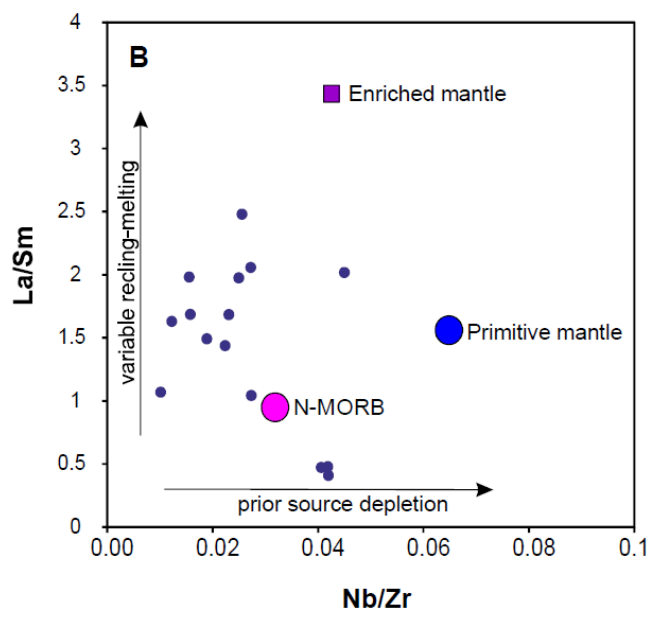
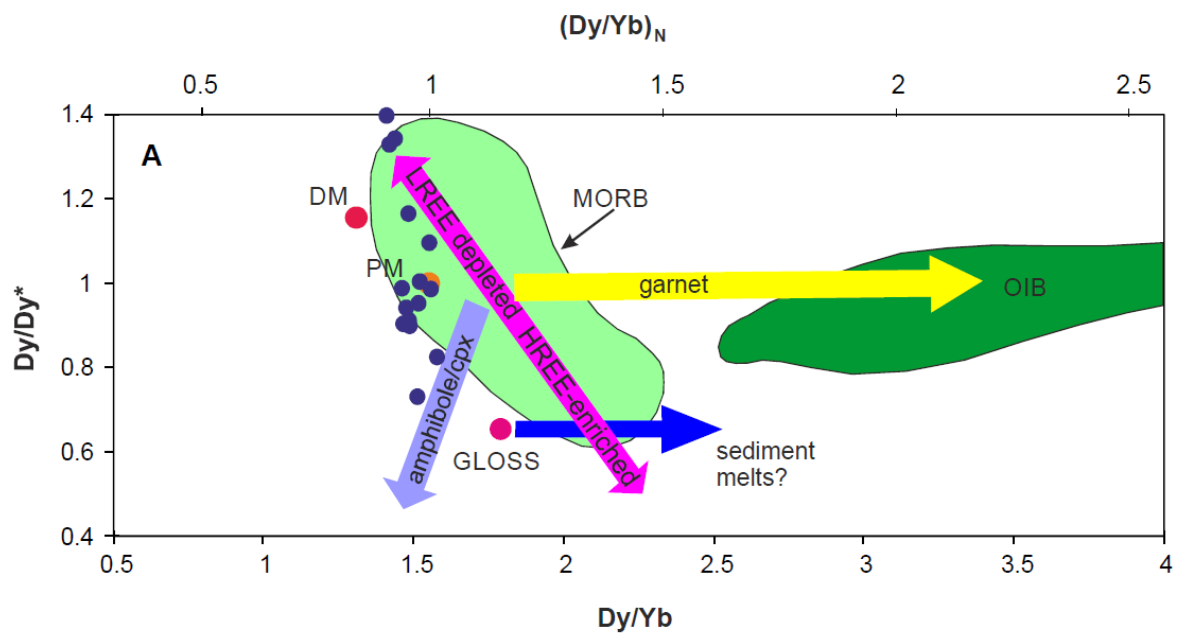


Fig.8

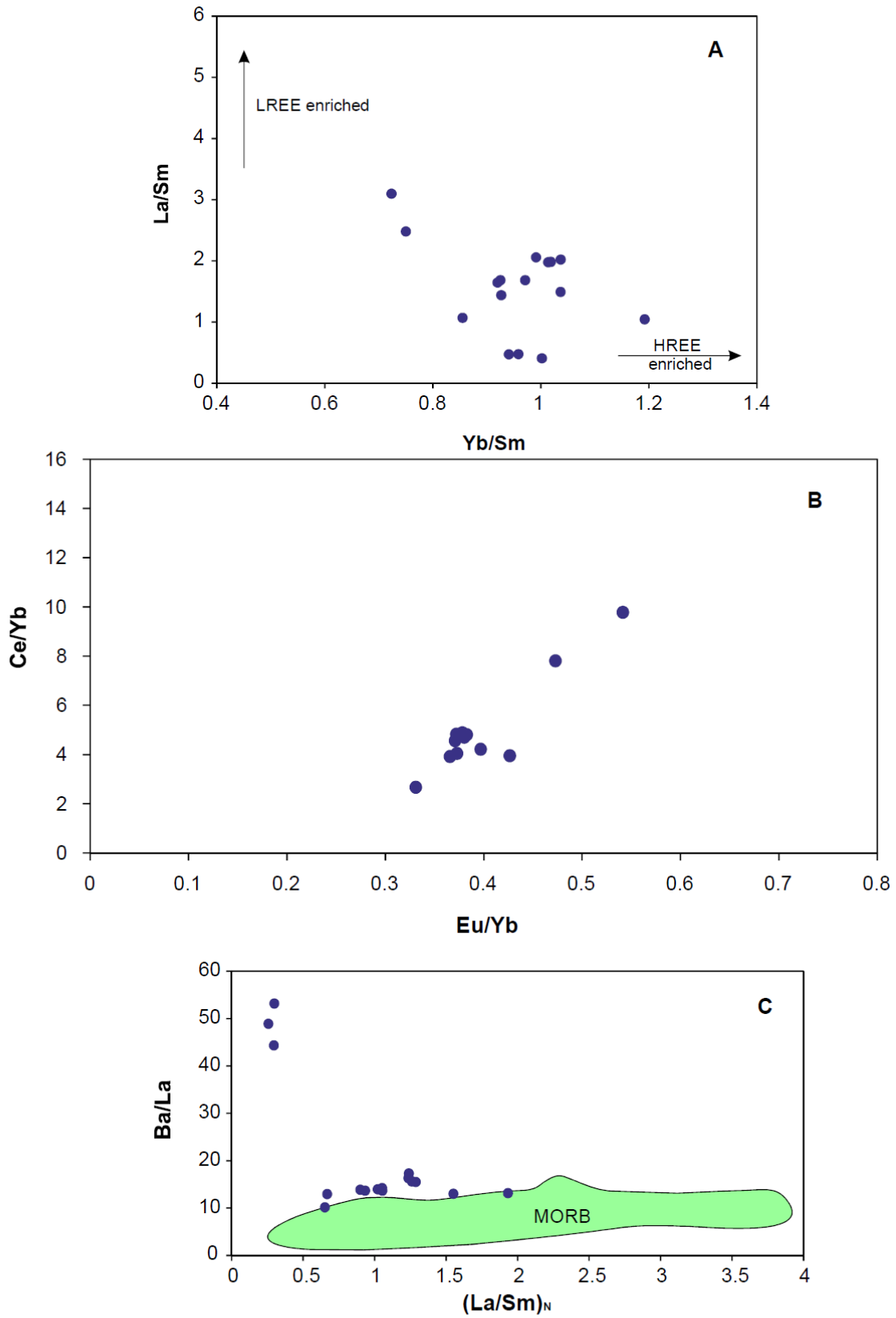


Fig. 9

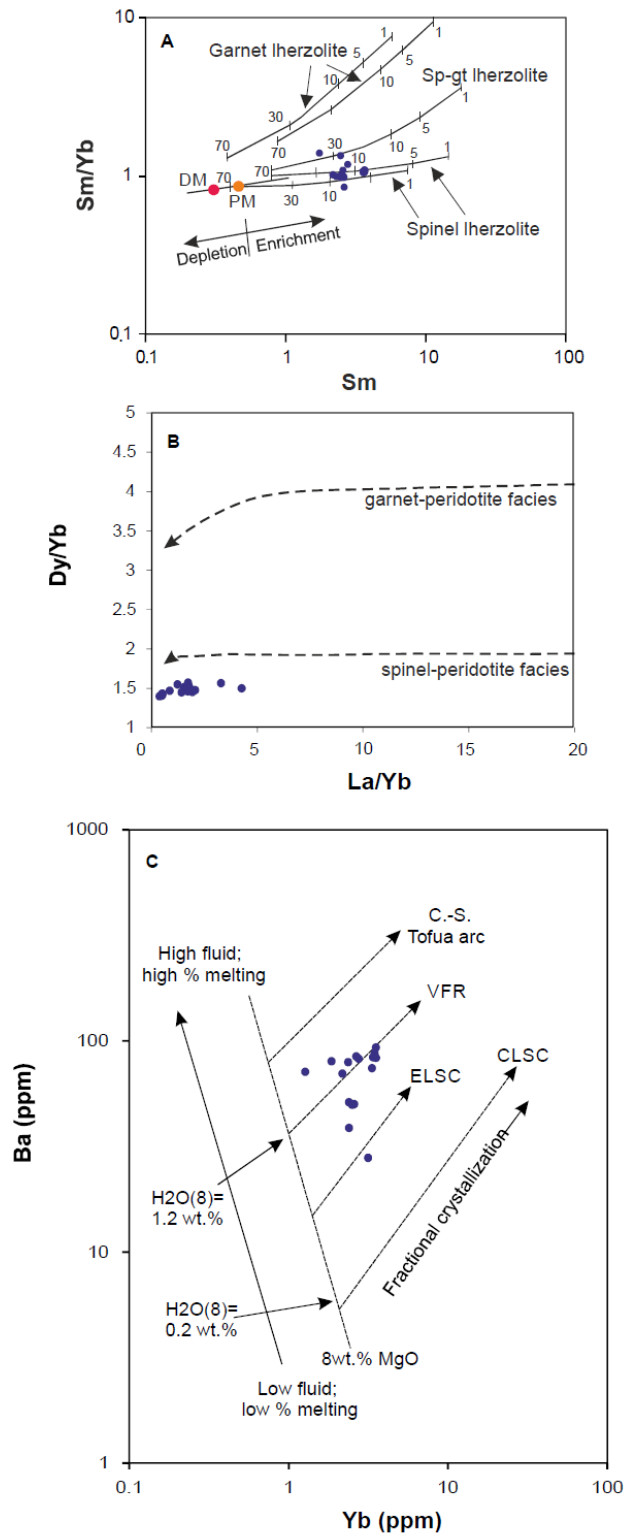


Fig.10

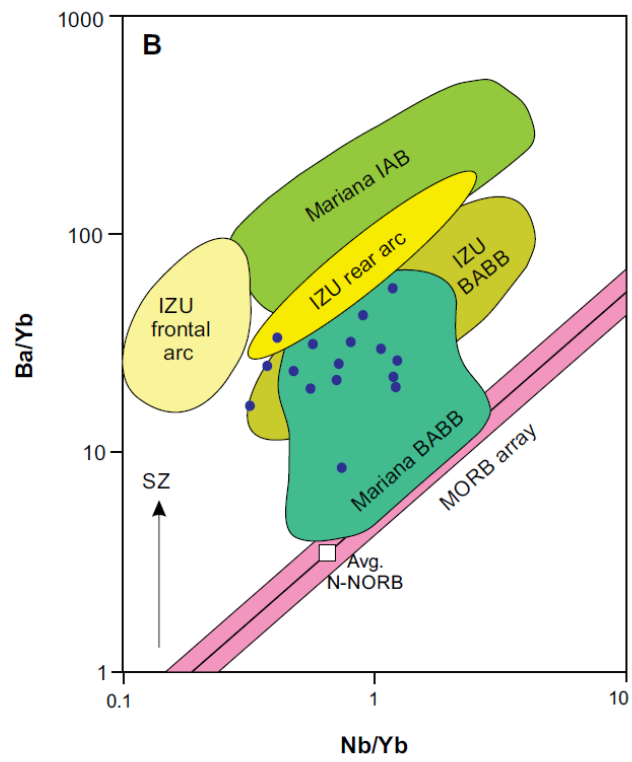
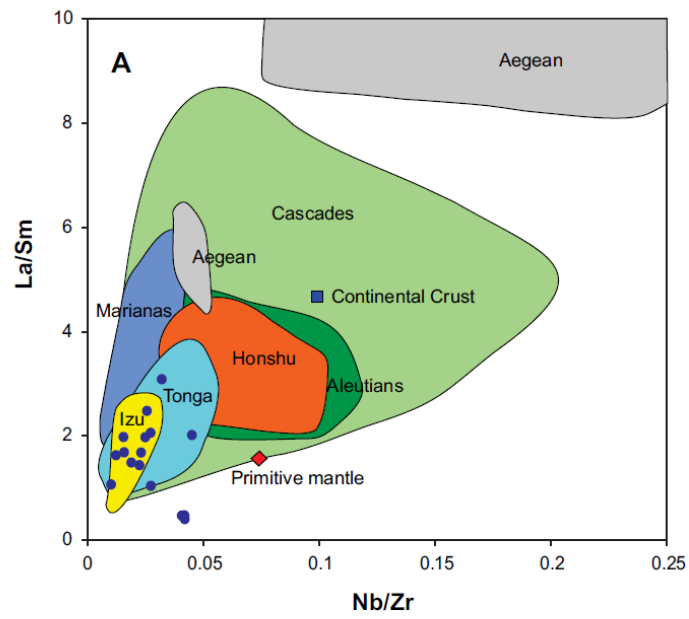


Fig.11

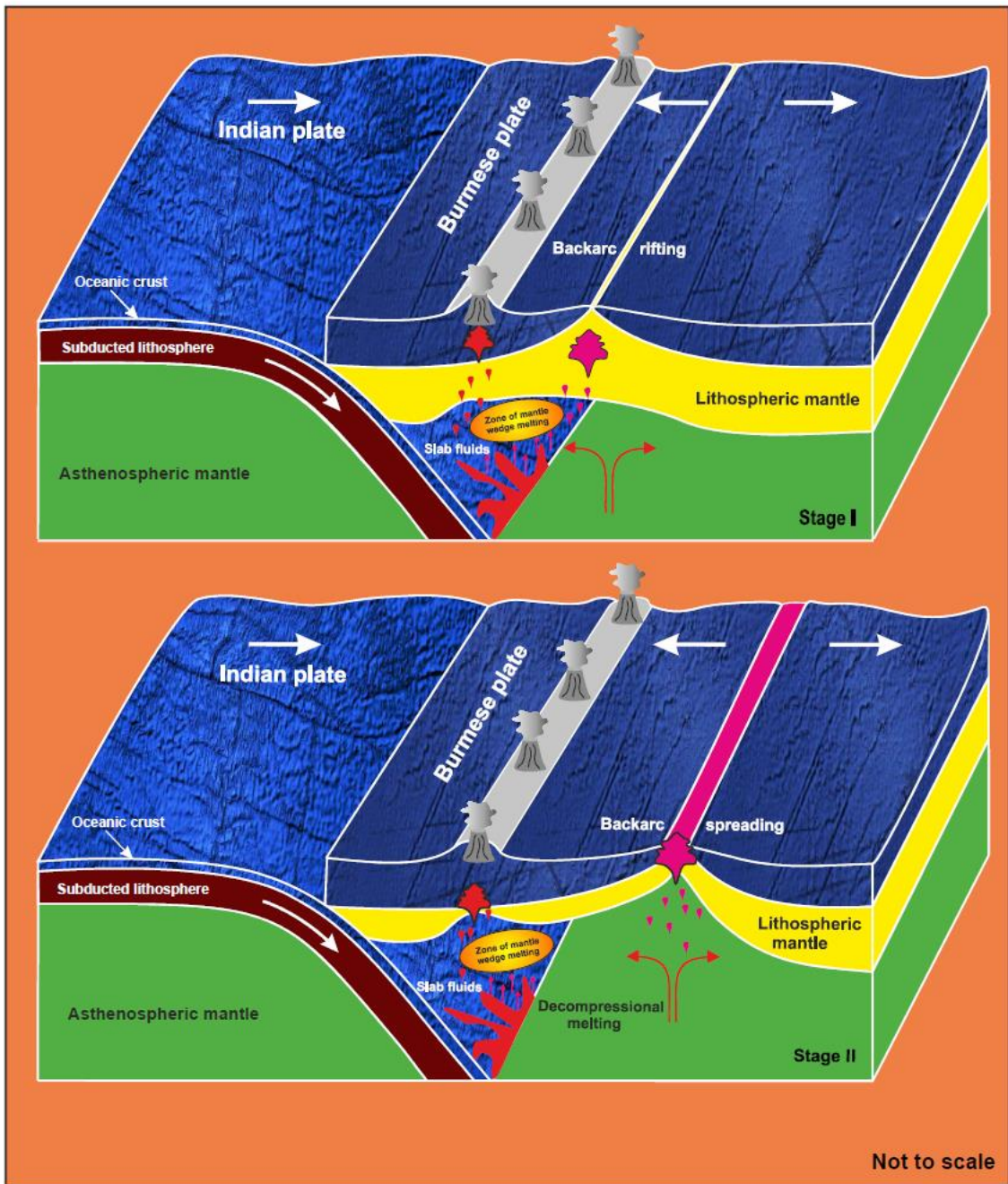


Fig.12

Table 1 Details of studied samples from Andaman backarc spreading centre

Dredge No	Cruise no and year	Depth (m)	Lat (N)	Long (E)	Megascopic Characters	*Microscopic Characters
D-8	MV AA Sidorenko-11, 1995	3765	10°20.736'	93°59.694'	fine grained and melanocratic	porphyritic in nature with zoned plagioclase, cpx and olivine phenocrysts
		3677	10°21.101'	94°00.183'		
D-9	MV AA Sidorenko-11, 1995	3386	10°24.308'	94°06.598'	vesicular, fine grained with Fe-Mn coating and melanocratic	porphyritic in nature with dominant zone plagioclase and cpx phenocrysts
		3353	10°24.512'	94°06.786'		
D-10	MV AA Sidorenko-11, 1995	2979	10°25.878'	94°09.571'	vesicular, fine grained to glassy and melanocratic	porphyritic in nature with dominant plagioclase and cpx phenocrysts with chilled margin
		2929	10°27.120'	94°09.570'		
D-11	MV AA Sidorenko-11, 1995	3346	10°32.408'	94°13.806'	very fine grained to with Fe-Mn coating and melanocratic	porphyritic in nature with dominant plagioclase and cpx phenocrysts with chilled margin
		3286	10°32.834'	94°14.577'		
D-16A	MV AA Sidorenko-11, 1995	3539	10°18.385'	93°54.422'	vesicular, fine grained and melanocratic	glomero-porphyritic in nature with dominant plagioclase and cpx phenocrysts
		3256	10°17.748'	93°54.592'		

*For petrographic details see Section 4

Table 2: Major and trace element composition of back arc basalts from Andaman subduction zone

Sample no.	D-10-1	D-10-2	D-10-3	D-8-1	D-8-2	D-8-3	D-9-1	D-9-2
<i>wt%</i>								
SiO ₂	50.80	50.30	50.12	49.71	48.83	52.09	49.60	52.73
TiO ₂	1.15	1.16	1.13	1.02	1.06	1.01	0.70	1.09
Al ₂ O ₃	16.95	18.85	19.10	17.93	17.48	14.34	17.44	16.80
Fe ₂ O ₃	2.65	2.66	2.63	2.52	2.56	2.51	2.20	2.59
FeO	7.45	7.09	7.03	5.62	5.67	5.70	6.49	7.17
MnO	0.16	0.16	0.16	0.15	0.15	0.15	0.15	0.16
MgO	5.90	5.22	5.17	7.85	8.13	8.29	7.52	5.40
CaO	10.09	9.98	10.27	11.14	11.18	10.26	12.13	9.55
Na ₂ O	2.59	2.97	3.16	2.92	2.90	2.77	2.19	2.71
K ₂ O	0.42	0.42	0.42	0.57	0.55	0.27	0.62	0.62
P ₂ O ₅	0.08	0.10	0.11	0.10	0.10	0.08	0.09	0.09
Total	98.24	98.91	99.30	99.53	98.61	97.47	99.13	98.91
Na ₂ O+K ₂ O	3.01	3.39	3.58	3.49	3.45	3.04	2.81	3.33
Mg#	38	36	36	50	51	51	47	36
<i>ppm</i>								
Sc	40	36	34	38	38	41	38	36
V	316	344	329	228	238	242	245	342
Cr	36	27	23	151	146	265	33	54
Co	187	177	146	143	165	111	166	186
Ni	16.8	9.9	9.8	93.3	95.9	93.0	43.8	16.3
Cu	72.5	47.2	47.2	60.4	67.7	63.0	93.6	71.1
Zn	71.2	77.5	72.7	69.4	66.9	71.9	64.0	76.9
Ga	12.0	11.6	10.9	8.7	11.1	10.8	12.2	11.0
Rb	6.8	7.7	5.5	5.1	5.0	4.2	9.3	7.4
Sr	167	173	170	150	148	144	333	166
Y	22.0	22.9	21.6	23.2	24.4	23.6	18.5	22.4
Zr	62.8	65.1	60.8	72.6	75.9	75.3	65.3	64.1
Nb	1.0	2.9	1.5	3.0	1.7	1.4	1.7	1.7
Cs	0.4	0.3	0.3	0.2	0.2	0.2	0.3	0.3
Ba	80	83	84	50	52	50	80	70
La	4.60	5.35	5.18	1.02	3.72	3.68	6.18	4.52
Ce	11.54	13.19	12.70	10.12	10.11	9.99	14.58	10.54
Pr	1.39	1.58	1.50	1.29	1.33	1.33	1.73	1.26
Nd	8.66	9.74	9.46	8.28	8.79	8.63	10.29	8.15
Sm	2.32	2.65	2.62	2.50	2.59	2.46	2.49	2.20
Eu	0.89	1.05	1.01	0.93	0.95	0.93	0.88	0.81
Gd	3.26	3.86	3.67	3.50	3.43	3.57	3.10	3.06
Tb	0.58	0.69	0.67	0.60	0.63	0.67	0.53	0.55
Dy	3.48	4.09	3.91	3.54	3.66	3.74	2.96	3.24
Ho	0.79	0.85	0.84	0.81	0.82	0.84	0.66	0.70
Er	2.43	2.91	2.78	2.56	2.53	2.58	1.95	2.32
Tm	0.42	0.49	0.47	0.44	0.43	0.47	0.33	0.40
Yb	2.36	2.75	2.66	2.50	2.40	2.55	1.87	2.18
Lu	0.36	0.42	0.41	0.35	0.37	0.40	0.27	0.36

Table 2: Contd...

Sample no.	D-10-1	D-10-2	D-10-3	D-8-1	D-8-2	D-8-3	D-9-1	D-9-2
(La/Sm) _N	1.24	1.26	1.24	0.26	0.90	0.93	1.55	1.29
(Ce/Yb) _N	1.32	1.30	1.29	1.09	1.14	1.06	2.11	1.31
(Dy/Yb) _N	0.99	1.00	0.99	0.95	1.02	0.98	1.06	1.00
(Gd/Yb) _N	1.14	1.16	1.14	1.16	1.18	1.16	1.37	1.16
Ti/Ti*	1.01	0.88	0.87	0.85	0.85	0.80	0.62	1.01
Ce/Ce*	1.12	1.11	1.12	2.17	1.11	1.11	1.09	1.08
Dy/Dy*	0.90	0.91	0.90	1.40	1.00	0.98	0.82	0.89
Zr/Y	2.86	2.84	2.81	3.13	3.11	3.19	3.53	2.86
Nb/Y	0.04	0.13	0.07	0.13	0.07	0.06	0.09	0.08
Zr/Sm	27.08	24.57	23.19	29.05	29.33	30.59	26.22	29.19
Nb/Zr	0.02	0.04	0.02	0.04	0.02	0.02	0.03	0.03
Nb/La	0.21	0.55	0.29	2.98	0.46	0.39	0.27	0.39
Zr/Nb	64.57	22.22	40.12	23.84	44.71	52.88	39.15	36.74
Nb/Yb	0.41	1.07	0.57	1.22	0.71	0.56	0.89	0.80
P/Nd	40.32	44.85	50.78	52.76	49.67	40.49	38.19	48.24

Normalization factors after Sun and McDonough
(1989)

Table 2: Contd...

Sample no.	D-11-1	D-16-A	D-16-A-2	D-16-A-3	D-16-A-5	D-16-A-6	D-16-A-7	D-16-A-4
<i>wt%</i>								
SiO ₂	49.83	55.75	51.65	51.95	51.38	45.78	48.50	51.12
TiO ₂	0.35	1.82	1.93	1.88	1.90	1.41	1.42	1.90
Al ₂ O ₃	18.19	13.21	15.05	15.06	16.98	16.77	16.18	17.13
Fe ₂ O ₃	1.85	3.32	3.43	3.38	3.40	2.91	2.92	3.40
FeO	5.76	8.21	8.36	8.25	7.74	7.64	6.84	7.96
MnO	0.14	0.17	0.17	0.22	0.17	0.16	0.15	0.17
MgO	7.50	5.10	5.19	5.12	4.32	8.51	9.10	4.64
CaO	12.47	7.09	7.69	7.53	7.59	11.88	10.81	7.69
Na ₂ O	2.13	3.07	3.48	3.27	3.95	2.56	2.87	3.97
K ₂ O	0.47	0.57	0.73	0.80	1.04	0.14	0.40	1.08
P ₂ O ₅	0.06	0.11	0.13	0.13	0.15	0.08	0.11	0.15
Total	98.75	98.42	97.81	97.59	98.62	97.84	99.30	99.21
Na ₂ O+K ₂ O	2.60	3.64	4.21	4.07	4.99	2.70	3.27	5.05
Mg#	50	31	31	31	29	45	49	30
<i>ppm</i>								
Sc	35	38	36	36	36	35	42	39
V	216	330	335	326	330	310	225	254
Cr	106	27	28	25	30	121	221	169
Co	191	166	158	176	157	135	176	124
Ni	48.1	8.7	6.7	8.9	6.2	100.3	131.1	151.3
Cu	96.4	51.0	51.3	55.7	49.2	58.1	91.7	70.1
Zn	54.6	93.0	99.9	97.4	89.7	96.6	91.7	82.1
Ga	10.2	13.6	13.9	11.1	13.3	10.0	11.3	11.4
Rb	5.9	8.8	9.0	9.0	12.0	11.3	1.0	3.9
Sr	339	158	173	166	164	159	146	165
Y	13.2	32.7	34.5	33.2	33.3	31.0	29.8	24.3
Zr	46.7	106.4	108.6	104.0	103.4	97.3	84.7	76.8
Nb	1.5	1.7	2.5	4.4	1.3	4.0	2.3	0.8
Cs	0.2	0.3	0.3	0.4	0.3	0.4	0.0	0.2
Ba	71	83	90	94	84	74	28	39
La	5.44	6.11	6.30	1.77	6.01	1.68	2.76	3.00
Ce	12.43	16.03	16.70	16.66	16.05	15.92	8.40	9.48
Pr	1.41	2.01	2.13	2.08	2.04	1.97	1.17	1.34
Nd	8.25	12.87	13.33	12.94	12.79	12.32	8.05	9.16
Sm	1.76	3.63	3.74	3.70	3.68	3.55	2.64	2.80
Eu	0.69	1.31	1.31	1.35	1.29	1.26	1.04	1.02
Gd	2.31	5.22	5.06	5.09	4.97	4.84	4.02	3.76
Tb	0.36	0.93	0.90	0.89	0.89	0.82	0.78	0.67
Dy	1.93	5.22	5.27	5.04	5.29	4.83	4.68	3.75
Ho	0.40	1.15	1.22	1.14	1.17	1.08	1.07	0.85
Er	1.34	3.62	3.61	3.65	3.57	3.45	3.36	2.52
Tm	0.22	0.63	0.62	0.63	0.61	0.58	0.57	0.43
Yb	1.27	3.52	3.46	3.54	3.39	3.34	3.15	2.40
Lu	0.21	0.54	0.53	0.52	0.51	0.48	0.48	0.34

Table 2: Contd...

Sample no.	D-11-1	D-16-A	D-16-A-2	D-16-A-3	D-16-A-5	D-16-A-6	D-16-A-7	D-16-A-4
(La/Sm) _N	1.93	1.05	1.05	0.30	1.02	0.30	0.65	0.67
(Ce/Yb) _N	2.64	1.23	1.30	1.27	1.28	1.29	0.72	1.07
(Dy/Yb) _N	1.02	0.99	1.02	0.95	1.05	0.97	1.00	1.05
(Gd/Yb) _N	1.50	1.23	1.21	1.19	1.21	1.20	1.06	1.30
Ti/Ti*	0.45	1.01	1.07	1.06	1.07	0.85	1.01	1.42
Ce/Ce*	1.10	1.12	1.12	2.13	1.12	2.15	1.15	1.16
Dy/Dy*	0.73	0.94	0.95	1.32	0.98	1.34	1.16	1.10
Zr/Y	3.53	3.25	3.14	3.14	3.10	3.14	2.84	3.17
Nb/Y	0.11	0.05	0.07	0.13	0.04	0.13	0.08	0.03
Zr/Sm	26.57	29.35	29.03	28.16	28.05	27.39	32.07	27.42
Nb/Zr	0.03	0.02	0.02	0.04	0.01	0.04	0.03	0.01
Nb/La	0.28	0.27	0.40	2.47	0.21	2.35	0.84	0.26
Zr/Nb	31.22	63.48	43.38	23.91	81.76	24.63	36.62	98.90
Nb/Yb	1.18	0.48	0.72	1.23	0.37	1.18	0.73	0.32
P/Nd	31.75	37.33	42.59	43.87	51.21	28.36	59.68	71.47

Normalization factors after Sun and McDonough
(1989)